Geobiology

WILEY

gebiology

ORIGINAL ARTICLE OPEN ACCESS

Untangling the Primary Biotic and Abiotic Controls on Oxygen, Inorganic and Organic Carbon Isotope Signals in Modern Microbialites

Robin Havas[1] | Christophe Thomazo[1,2] | Jeanne Caumartin[3,4] | Miguel Iniesto[4] | Hugo Bert[5] | Didier Jézéquel[6] | David Moreira[4] | Rosaluz Tavera[7] | Vladimir Bettencourt[7] | Purificación López-García[4] | Emmanuelle Vennin[1] | Karim Benzerara[3]

[1]Biogéosciences, UMR CNRS EPHE, Université de Bourgogne, Dijon, France | [2]Institut Universitaire de France, Paris, France | [3]Museum National d'Histoire Naturelle, UMR CNRS 7590, Institut de Minéralogie, de Physique Des Matériaux et de Cosmochimie (IMPMC), Sorbonne Université, Paris, France | [4]Unité d'Ecologie Systématique et Evolution, CNRS, Université Paris-Saclay, AgroParisTech, Orsay, France | [5]ENS de Lyon, Laboratoire de Géologie de Lyon: Terre, Planètes, et Environnement, CNRS, UMR 5276 LGL-TPE, Université Claude Bernard Lyon 1, Villeurbanne, France | [6]IPGP, CNRS UMR 7154, Université de Paris & UMR CARRTEL, INRAE-USMB, France | [7]Departamento de Ecología y Recursos Naturales, Universidad Nacional Autónoma de Mexico, Mexico City, DF Mexico, Mexico

Correspondence: Robin Havas (robin.havas@gmail.com)

Received: 8 September 2024 | **Revised:** 11 December 2024 | **Accepted:** 27 January 2025

Funding: This research was supported by the Agence Nationale de la Recherche (France, grant no. ANR-18-CE02-0013-02). Jeanne Caumartin was funded by a grant from the Interface pour le vivant doctorate programme at Sorbonne Université.

Keywords: carbonate geochemistry | microbialite | modern analogue

ABSTRACT

Microbialites are organo-sedimentary structures formed throughout most of the Earth history, over a wide range of geological contexts, and under a multitude of environmental conditions affecting their composition. The carbon and oxygen isotope records of carbonates, which are most often their main constituents, have been used as a widespread tool for paleoenvironmental reconstructions. However, the multiplicity of factors that influence microbialites formation is not always properly distinguished in their isotopic record, in both ancient and modern settings. It is therefore crucial to refine our understanding of the processes controlling microbialites isotopic signal. Here, we analyzed the carbon and oxygen isotope compositions from bulk and micro-drilled carbonates as well as bulk organic carbon isotope compositions in microbialites from four Mexican volcanic crater lakes of increasing alkalinity. The survey of four lakes allows comparing microbialite formation processes and their geochemical record within distinct physico-chemical contexts. The geochemical analyses were performed in parallel to petrographic and mineralogical characterization and interpreted in light of the known microbial community composition for microbialites of the same lakes. Combining these data, we show that the potential for isotopic biosignature preservation primarily depends on physico-chemical conditions. Carbon isotope biosignatures pointing out to an autotrophic influence on carbonate precipitation are preserved in the lowest alkalinity lakes. By contrast, higher alkalinity lakes, where microbialites are more massive, favor carbonate precipitation in isotopic equilibrium with the lake water, with secondary influence of heterotrophic organic carbon degradation. From these results, we suggest that microbialite carbonate C isotope records can be interpreted as the balance between the microbialite net primary productivity and the amount of precipitation that relates to physico-chemical forcing. The signals of microbialite oxygen isotope compositions highlight a lack of understanding in the oxygen isotope records of relatively rare carbonate phases such as hydromagnesite. Nonetheless, we show that these signals are primarily influenced by the basins' hydrology, though biological effects may also play a (minor) role. Overall, both carbon and oxygen isotopic signals may record a mixture of different local/

---

global and biotic/abiotic phenomena, making microbialites intricate archives of their growth environment, which should thus be interpreted with cautions and in the light of their surrounding sediments.

1 | Introduction

Microbialites are organo-sedimentary structures forming through the interaction of biotic and abiotic factors (Burne and Moore 1987). As such, they represent emblematic objects in geobiology, extensively used as paleoenvironmental archives (e.g., Frantz et al. 2014; Hren and Sheldon 2020; Lepot 2020; Hohl and Viehmann 2021; Vignale et al. 2021; Antunes et al. 2022). Microbialites contain a broad diversity of morphological, mineralogical, microbiological, and geochemical signatures, as a result of the myriad of environmental factors that influence their formation (e.g., Riding 2006, 2011; Della Porta 2015; Chagas et al. 2016; Grey and Awramik 2020; Vennin et al. 2019, 2021; Iniesto, Moreira, Reboul, et al. 2021; Zeyen et al. 2021). Accordingly, they are studied by a wide range of techniques and disciplines. Among these, isotope geochemistry, especially that of carbon, is responsive to biological and abiotic environmental constraints, and to both very local (e.g., metabolic activity) and large-scale (e.g., climate, hydrology) processes that impact microbialite formation (e.g., Chagas et al. 2016). Carbonate minerals, which have been particularly studied in Earth sciences, are most often the main constituents of microbialites, and thus represent primary targets for studying these archives.

The carbonate $\delta^{13}C$ signal of microbialite-hosting sedimentary sequences has been used to reconstruct C cycle changes from the basin- to the global-scale back to the Late Archean (e.g., Fischer et al. 2009; Chakrabarti et al. 2011). At a smaller scale, $\delta^{13}C$ and $\delta^{18}O$ isotopic compositions of microbialitic carbonates have been used to discuss the specific influence of autotrophic or heterotrophic organisms, and evaporative conditions on microbialite formation from the Paleogene (Frantz et al. 2014), Cretaceous (Bahniuk et al. 2015) or Permian (e.g., Friesenbichler et al. 2018; Zhang et al. 2021; Antunes et al. 2022) periods, back to the Proterozoic (Khelen et al. 2017; Zhu et al. 2021) and Archean (Xu 2011) Eons. However, a proper understanding of the isotope transfer functions from the environment to the microbialites in modern analogous systems is mandatory in order to meaningfully interpret the ancient record, especially considering the multiplicity of factors that may be involved in microbialite formation and that the variations usually discussed in the literature are relatively small (Houghton et al. 2014; Della Porta 2015).

Carbonate isotopic signatures in microbialites from recent Quaternary to the present have been increasingly suggested to faithfully archive environmental parameters such as temperature, hydrological balance, or the influence of external fluid sources (Newell et al. 2017; Buongiorno et al. 2018; Arenas et al. 2019; Bougeault et al. 2020). Additionally, combining the isotopic signatures of carbonates and organic C, different studies on modern microbialites evidenced a predominant influence of autotrophic (Louyakis et al. 2017; White III et al. 2020; Ingalls et al. 2020, 2024), heterotrophic (Andres et al. 2006; Breitbart et al. 2009; Pace et al. 2016) or both types of metabolisms (Nitti et al. 2012) on carbonate formation. However, it is not understood why these metabolic groups influencing carbonatogenesis differ from one microbialite to another, and why they are more or less expressed in the microbialite carbonate isotopic signatures. These studies on modern systems also mostly focus on single locations, often corresponding to hypersaline contexts, and it remains to be assessed how distinct environmental contexts may differently affect the microbialite isotopic signals, especially considering the intertwined influence of biotic and abiotic factors on microbialite formation. Focusing on the Great Salt Lake, Ingalls et al. (2020) showed for instance that the isotopic record of distinct carbonate facies within a single setting were heterogeneously sensitive to biotic and abiotic constraints. Therefore, a more integrated approach and understanding of microbialite isotopic signatures comparing several contexts, and considering both biotic and abiotic factors is still required.

Here, we investigated four alkaline and redox-stratified lakes in Mexico, showing diverse hydrochemistry and physico-chemical parameters, notably salinity and alkalinity, and hosting microbialites with diverse mineralogical and microbial community compositions. In particular an inter-lake alkalinity gradient was found with the minimum alkalinity measured in Lake Alberca de los Espinos (~7.5 mM) and the highest alkalinity in Lake Alchichica (~45 mM). The parameters and processes influencing the formation of microbialites in these lakes were previously explored using elemental geochemistry, mineralogical and metabarcoding analyses (Saghaï et al. 2015; Valdespino-Castillo et al. 2018; Iniesto, Moreira, Reboul, et al. 2021; Zeyen et al. 2015, 2019, 2021). Nonetheless, isotopic signatures of these microbialites remain virtually unexplored except for a few carbonate C and O isotope measurements from Lake Alchichica (Kaźmierczak et al. 2011). In the present study, we systematically characterized the mineralogical and isotope signatures of both carbonates and organic carbon in microbialites across the inter-lake alkalinity gradient. We also measured the isotopic signatures of the lakes water and dissolved inorganic carbon in order to assess whether the microbialites precipitated in isotopic equilibrium with their environment or not and which processes mostly influence their formation and isotopic record. Additionally, we analyzed some of the groundwater feeding the lakes in order to trace possible source effects. Overall, this provides the opportunity to assess the sensitivity of microbialite carbonate isotopic records to distinct water chemistries, hydrological contexts, mineralogical assemblages, and biological influences from various environmental contexts. Interestingly, the microbialites studied here may be compared with the ancient microbialite record, assumed to have predominantly formed by authigenic mineral precipitation (Grotzinger 1990; Corkeron et al. 2012).

2 | Geological Setting and Sample Description

2.1 | Geological Context

The microbialites were collected in four lakes located in tuff cones and maar craters. All these craters belong to the Trans-Mexican Volcanic Belt (TMVB; Figure 1). The TMVB extends

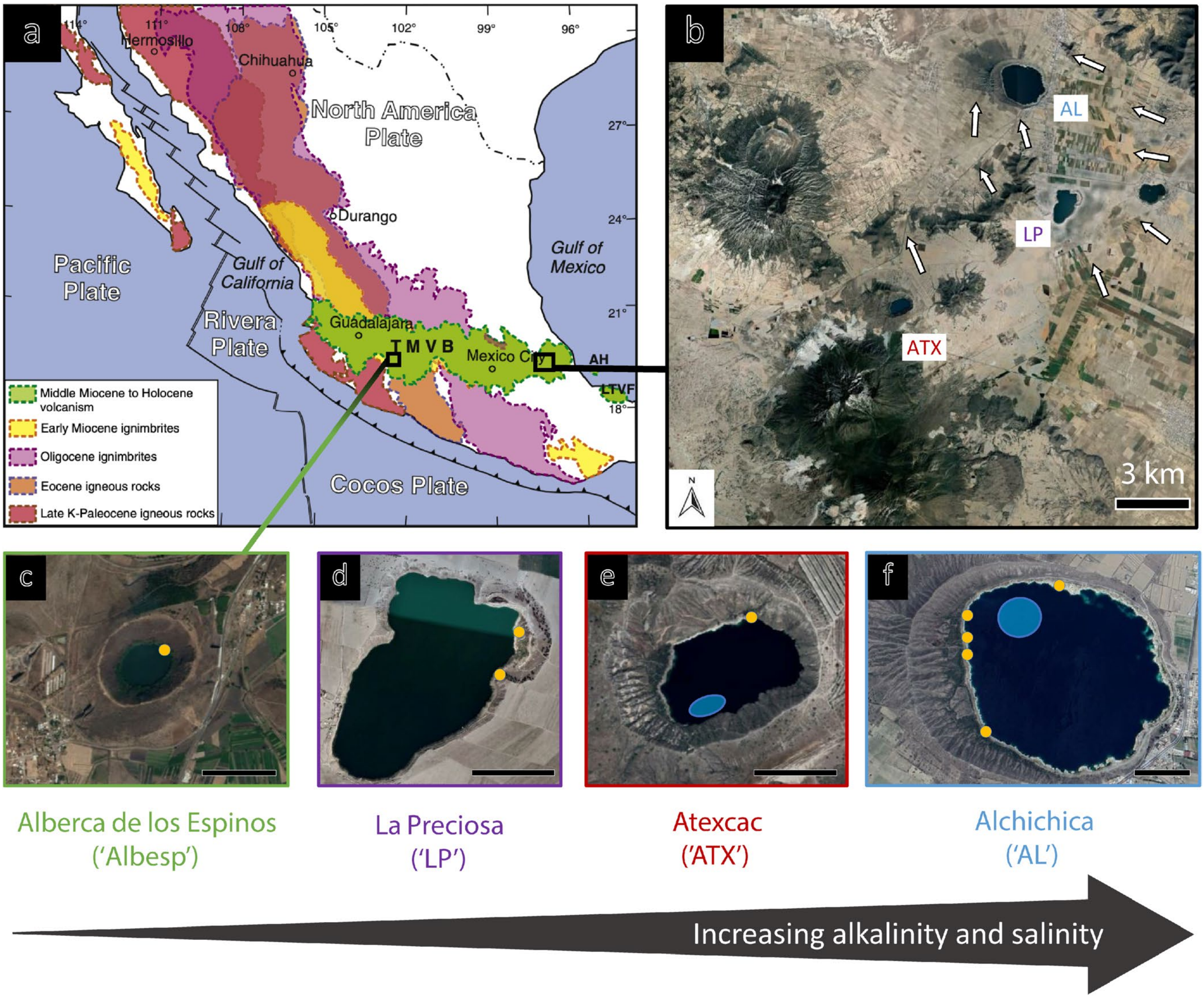

FIGURE 1 | Geographical location and photographs of the four crater lakes. (a) Geological map from Ferrari et al. (2012), with black squares showing the location of the four studied lakes within the Trans-Mexican Volcanic Belt (TMVB). (b) Close up ©Google Earth views of the lakes La Preciosa, Atexcac, and Alchichica in the Serdán-Oriental basin (SOB). The white arrows in (b) represent the approximate groundwater flow path (based on Silva Aguilera 2019). (c–f) Close up ©Google Earth views of each individual lake with black scale bars representing 500 m. Blue areas in Atexcac (e) and Alchichica (f) represent the zones where deep microbialites (between 5 and 20 and 5 and 10 m, respectively) were sampled by scuba divers. Yellow dots represent the locations where emerged or slightly immersed microbialites were hand sampled. The black arrow represents the inter-lake alkalinity and salinity gradient direction.

along an E-W direction in central Mexico, over a distance of ~1000 km, and a width of ~90–230 km (Ferrari et al. 2012). It is related to the subduction of the Cocos and Rivera plates under the North American plate, and contains a few dozens of stratovolcanoes, large caldera complexes, hundreds of domes and shield volcanoes, and > 3000 small monogenetic volcanoes such as scoria cones, tuff cones, and maars (Kshirsagar et al. 2016 and references therein). Tuff cones and maar craters form when ascending magma meets water-saturated substrates, leading to successive explosions and the excavation of volcanic, and older country-rock material (Lorenz 1986; Carrasco-Núñez et al. 2007; Siebe et al. 2012; Chako Tchamabé et al. 2020).

Lake Alberca de los Espinos is located within the vast monogenetic Michoacán-Guanajuato volcanic field (MGVF), in the central-western part of the TMVB (Figure 1). The lake infills a tuff cone volcano, formed in a highly faulted area at the margin of the Zacapu tectonic lacustrine basin (Siebe et al. 2012). The crater itself lies on a normal fault, at a current altitude of ~1985 m above sea level (masl), and was dated at ~25 ± 2 ka (Siebe et al. 2012, 2014). The geological basement is mainly composed of basaltic andesite, andesite, and dacite rock types (Siebe et al. 2012; Kshirsagar et al. 2016).

La Preciosa, Atexcac, and Alchichica are three maar lakes in the easternmost part of the TMVB, found within an intra-mountain closed basin called the Serdán-Oriental Basin (SOB). The three lakes are located less than 10 km away from each other, at an average altitude of about 2300 masl (Figure 1). The SOB geological basement is composed of folded and faulted Cretaceous limestone and shales, covered by andesitic to basaltic lava flows (Carrasco-Núñez et al. 2021). The crater in La Preciosa was not

TABLE 1 | General information of the studied lakes.

Lake	General location	Location	Elevation (masl)	Lake basement	Age (ka)	Max depth (m)	Area (km^2)
Alberca de los Espinos	Zacapu Basin, MGVF, central TMVB	19°54′23.9″ N; 101°46′07.8″ W	1985	Andesites	25 ± 2	30	~0.1
La Preciosa	Serdán-Oriental Basin, eastern TMVB	19°22′18.1″ N; 097°23′14.4″ W	2330	Limestone, andesites, basalts	Holocene	46	~0.8
Atexcac	Serdán-Oriental Basin, eastern TMVB	19°20′2.2″ N; 097°26′59.3″ W	2360	Limestone, andesites, basalts	8.3-5.1 ± 0.1-0.2	39	~0.3
Alchichica	Serdán-Oriental Basin, eastern TMVB	19°24′51.5″ N; 097°24′09.9″ W	2320	Limestone, andesites, basalts	6-13 ± 5-6	62	~2.3

Lake	Alkalinity (mM)[a]	Salinity (psu)[a]	pH[a]	Microbialites description
Alberca de los Espinos	~7	0.6	9.14	Thin living microbialites, encrusting basalts
La Preciosa	~13.5	1.15	9.01	Living microbialites, sporadic non-living microbialites around the crater
Atexcac	~26	7.4	8.85	Well-developed living microbialites, thick non-living microbialites covering the crater walls
Alchichica	~35	7.9	9.22	Well-developed living microbialites, large non-living microbialite reefs

Abbreviations: masl, Meters above sea level; MGVF, Michoaćan-Guanajuato volcanic field; TMVB, Trans-Mexican volcanic belt.
[a] Values from May 2019.

dated but is likely Holocene in age (Carrasco-Núñez et al. 2021). The formation of Atexcac crater was dated between 8.3 and 5.1 ka (Chédeville et al. 2020). Alchichica crater was dated between 6 and 13 ka (Chako Tchamabé et al. 2020; Chédeville et al. 2020) (Table 1).

2.2 | Geochemical and Limnological Context

The four lakes are warm monomictic: they are stratified for about 9 months of the year and mix only when the thermal stratification breaks down during winter (Armienta et al. 2008; Rendon-Lopez 2008). The four lakes are closed lakes, that is, with no surface inflow or outflow, and their global water chemistry is mainly influenced by the chemical composition of infilling groundwater, and by the ratio between precipitation and evaporation fluxes (Silva-Aguilera et al. 2022). They all have $DIC/(Ca^{2+} + Mg^{2+})$ ratio above unity and an evaporation rate higher than precipitation (Kshirsagar et al. 2015; Silva-Aguilera et al. 2022). This leads to high pH values around 9 (Pecoraino et al. 2015; Zeyen et al. 2021). Nonetheless, the four lakes exhibit contrasted water chemical compositions due to specific differences in geological, climatic, and limnologic contexts (Zeyen et al. 2021; Havas et al. 2023a). In particular, they follow a gradient of water chemistries with parameters such as dissolved Mg/Ca ratio, alkalinity, salinity, and sulfate concentrations increasing in this order: Alberca<La Preciosa<Atexcac < Alchichica (Zeyen et al. 2021; Figure 1).

Dissolved inorganic carbon concentration ([DIC]) follows the same gradient as it correlates with alkalinity (Havas et al. 2023a). Havas et al. (2023a) the processes generating the alkalinity gradient also control the DIC isotope composition in the lakes ($\delta^{13}C_{DIC}$), with average values increasing from −3‰ in Alberca to +2‰ in Alchichica. In brief, Lake Alberca isotopic signatures are lower than in the SOB lakes notably because it evolves under a more humid and less evaporative context. Besides, the groundwater feeding the lakes in the SOB likely contain a higher alkalinity/DIC content due to the presence of limestone in the basement. Hence, the DIC reservoir in Lake Alberca has a higher sensitivity to organic matter respiration (and potentially volcanic degassing) decreasing its $\delta^{13}C_{DIC}$ (Havas et al. 2023a). The isotopic differences among the SOB lakes likely arise from the specific flowpath of the groundwater, and possibly small-scale variations in volcanic degassing and climatic conditions (Lelli et al. 2021; Havas et al. 2023a). The $\delta^{13}C_{DIC}$ trend between the four lakes was reflected in the surficial sediment carbonates at the bottom of the lakes, as they also record increasing $\delta^{13}C_{carb}$ from about −1.5‰ in Alberca to 4.6‰ in Alchichica (Havas et al. 2023a).

2.3 | Microbialite Distribution, Main Mineralogical and Microbial Characteristics

Microbialites are found in the four lakes and increase in abundance from lower (Alberca) to higher (Alchichica) alkalinity conditions (Iniesto, Moreira, Reboul, et al. 2021; Zeyen et al. 2021). Their mineralogy also significantly changes depending on each lake's chemistry (Zeyen et al. 2021).

In Alberca de los Espinos, microbial deposits are scant and consist of decimeter-sized submerged and emerged microbial crusts and columns; they concentrate on the western shore of the lake (Zeyen et al. 2019; Figure 2). Their mineralogical assemblage mainly consists of monohydrocalcite and Mg-calcite, together

FIGURE 2 | Distribution and representative pictures of the microbialites macro- and mega-structures in the four Mexican lakes. The lake physiography and microbialite abundance markedly differ from one lake to the other. In Atexcac, the series of 'ATX-C' samples discussed in the text correspond to microbialites emerged from ~1 to 6 m (yellow arrow) with close-up images located thanks to white and red dots. In the Alchichica panel, the blue and brown labels refer to the "white" and "brown" microbialite facies, respectively. Brown microbialites are found specifically on the western side of the lake whereas white microbialites form all around it. Immerged white microbialites such as 'AL-R-2' and 'AL19-5m' appear fully white beneath the colored surface-active photosynthetic layer. White scale bars on microbialite pictures represent 1 cm.

with Mg-silicate phases such as kerolite and/or stevensite (Zeyen et al. 2019, 2021).

In La Preciosa, microbialites mainly spread on the few prominent hard surfaces of the crater walls all around the lake but also form steep bioherms on the northern shore of the lake (Figure 2). Microbialites can be found up to 6–7 m above the current water level. They harbor more or less eroded clotted surfaces typical of thrombolites, and sometimes shrubs typical of dendrolites, with detrital particles infilling the voids (Figure 2; Grey and Awramik 2020). La Preciosa microbialites are dominated by aragonite and a poorly crystalline Mg-silicate phase similar to kerolite, with minor amounts of calcite (Zeyen et al. 2015).

Atexcac crater is steep and microbialites mostly develop as large encrustations and mounds capping the crater walls all around the lake but its western flank, where the lake is bordered by a gentler sandy beach portion (Figure 2). At the mesoscale, samples underwater or emerged (up to ~11 m above the current water level) harbor more or less eroded mesoclots typical of thrombolites (Grey and Awramik 2020), but appear structure-less below the surficial crust. Atexcac microbialites are mainly composed of aragonite and kerolite, with minor amounts of calcite and hydromagnesite as well as significant amounts of amorphous silica from diatoms (Zeyen et al. 2015, 2021).

In Alchichica, microbialites constitute a large carbonate platform visible all around the lake (Figure 2). Massive bioherms emerge up to ~5 m above the current water level and are found at depths down to at least 15 m (Saghaï et al. 2016). Alchichica microbialites can be broadly categorized in two main groups: (i) white cauliflower-shaped microbialites located all around the lake and composed mainly of hydromagnesite, and aragonite at their surface; (ii) brown/orange columnar microbialites only located on the western shore and composed mostly of aragonite (e.g., Kaźmierczak et al. 2011; Valdespino-Castillo et al. 2014; Zeyen et al. 2019). For simplicity, we will refer to these two main microbialite categories as the “white” and “brown” facies. Mesoclots typical of thrombolites can be found in some of the submerged samples (all belonging to the white facies) but quickly disappear into a structure-less carbonate matrix below the microbialites' surface (Figure 2). Microbialites from the second group (brown facies) were mainly structure-less at the mesoscale; some were characterized by a macro-porosity caused by insect-nests and/or aquatic vascular plants.

Although the microbial communities composing the microbialites of the different lakes vary across the previously described alkalinity gradient, they share a common core of prokaryotic and eukaryotic members (Iniesto, Moreira, Reboul, et al. 2021). This core microbiome comprising oxygenic and anoxygenic photosynthesizers (primarily cyanobacteria, Chloroflexi, Rhodobacteriales, Rhodospirilalles, and Chromatiaceae) suggests that some of these microorganisms are key in the formation of the Mexican microbialites, with microbial sulfate reduction (MSR) having only a minor contribution in these systems (Saghaï et al. 2015, 2016; Valdespino-Castillo et al. 2018; Iniesto, Moreira, Reboul, et al. 2021). The core microbiome also includes typical EPS-degrading taxa (aerobic heterotrophs from the Bacteroidetes and Planctomycetes groups; EPS for extracellular polymeric substances). We note that eukaryotes represent a minor fraction of the microbialite communities (~5%–10%).

3 | Methods

3.1 | Field Work and Sampling

The majority of microbialites and lake waters were sampled in May 2019 (Table 2). Abbreviations ‘Albesp’, ‘LP’/‘PR’, ‘ATX’, and ‘AL’ refer to samples from lakes Alberca de los Espinos, La Preciosa, Atexcac, and Alchichica, respectively. Water samples were collected at different depths using a Niskin bottle, and filtered at 0.22 μm with pre-ashed Filtropur S filters (rinsed with lake water) for analyses of dissolved inorganic carbon (DIC), major, minor, and trace ions (Havas et al. 2023a). Groundwater in the SOB was sampled in October 2022, directly coming out of the pumping pipes of farming wells. Water samples were filtered at 0.22 μm with pre-ashed Filtropur S filters directly after collection for dissolved element concentrations and DIC isotope measurements. Microbialites from the lake shores and crater rims were sampled both above and below water surface (as “subfossil” and “active” microbialites, respectively). “Active” microbialites were also collected by scuba divers at depths from 5 to 20 m in Atexcac, and from 5 to 10 m in Alchichica (Table 2). Here, by “active” microbialites, we mean microbialites that are still underwater and covered by an actively growing/living microbial mat as evidenced by the presence of fresh organic mats on the microbialites.

3.2 | Mineralogical Analyses

Mineralogical assemblages were determined by X-ray diffraction (XRD) analyses of bulk powders at the Laboratoire Biogéosciences (GISMO platform, Dijon). Samples were ground in an agate mortar. Diffractograms were measured with a Bruker D8 Endeavor diffractometer using the Cu Kα radiation and a LynxEye XE-T detector, operated at 40 kV and 25 mA intensity. Mineral identifications were based on COD (“Crystallography Open Database”) and BGMN databases. Estimation of mineral abundances was achieved using a Rietveld refinement analysis implemented in the Profex software (Döbelin and Kleeberg 2015). The goodness of fit was assessed by the χ^2 parameter for each Rietveld refinement analysis (Table S1; examples). Examples of sample and fitting diffractograms are shown in Figure S1.

3.3 | Microscopy Analyses

Thin sections prepared by “Lithologie Bourgogne” (Dijon, France) were examined using a Nikon AZ100 optical microscope in order to determine the lithology and sedimentary facies of the microbialites. The thin sections were observed under plane-polarized light and cross-polarized light and images were recorded with a Tucsen TrueChrome 4K Pro camera (GISMO platform, Dijon). Additionally, UV-epifluorescence microscopy was carried out on the Nikon AZ100. Last, elemental mapping was carried out on entire thin sections using a micro x-ray fluorescence 2D scanner (Bruker M4 Tornado) composed of two silicon drift detectors, a Cr x-ray tube anode and a polycapillary lens providing a 25 μm lateral resolution (GISMO platform,

TABLE 2 | Main sampling and classification information about the microbialites studied. The detailed characteristic of the facies groups are presented in the main text.

Sample name	Latitude	Longitude	Sampling date	Underwater // Subfossil (oxygen conditions)	Depth/height relative to current water level (m)	Facies group	Main carbonate mineralogy
AL19-mb-5m	19°25′10″ N	97°24′22″ W	05/21/2019	Underwater (oxic)	−5	White	Hmg, Ara
AL19-mb-10m	19°25′10″ N	97°24′22″ W	05/21/2019	Underwater (oxic)	−10	White	Hmg, Ara
AL-T-1	19°25′5.2″ N	97°24′41.1″ W	05/24/2019	Subfossil	≈ +2	White	Hmg, Ara
AL-T-5	19°24′59.1″ N	97° 24′40.9″ W	05/24/2019	Subfossil	≈ +2	Brown	Ara
AL-T-6	//	//	05/24/2019	Subfossil	≈ +2	White	Hmg, Ara
AL-T-7	19°24′58.3″ N	97°24′40.7″ W	05/24/2019	Subfossil	≈ +2	White	Hmg, Ara
AL-T-8	//	//	05/24/2019	Subfossil	≈ +2	Brown	Ara
AL-T-9	19°24′56.9″ N	97° 24′40.5″ W	05/24/2019	Subfossil	≈ +2	Brown	Ara
AL-T-10	19°24′55.1″ N	97°24′40.1″ W	05/24/2019	Subfossil	≈ +2	Brown	Ara
AL-T-11	//	//	05/24/2019	Subfossil	≈ +2	White	Hmg, Ara
AL-R-1	19°25′14.0″ N	97°24′12.9″ W	05/21/2019	Subfossil	0	White	Hmg, Ara
AL-R-2	//	//	05/21/2019	Underwater (oxic)	0	White	Hmg, Ara
AL-R-3	//	//	05/21/2019	Subfossil	≈ +0.5	White	Hmg, Ara
AL-R-4	19°25′14.0″ N	97°24′14.5″ W	05/21/2019	Subfossil	≈ +1	White	Hmg, Ara
AL-R-5	19°25′15.1″ N	97°24′14.7″ W	05/21/2019	Subfossil	≈ +4	White	Hmg, Ara
Al-Fe-W	19°24′59.10″N	97°24′40.79″W	05/24/2019	Subfossil	≈ +2	Brown	Ara
AL22-mb-Sb	19°24′32.5″ N	97°24′33.4″ W	10/28/2022	Underwater (oxic)	−0.5	Brown	Ara
LP-50cm	19°22′12.7″ N	97°23′1.3″ W	05/24/2019	Underwater (oxic)	−0.5	LP	Ara
PR-1	19°22′20.9″ N	97°22′57.4″ W	05/24/2019	Subfossil	≈ +3	LP	Ara
PR-2	19°22′12.7″ N	97°23′1.3″ W	05/24/2019	Subfossil	0.5	LP	Ara
PR-3	19°22′18.7″ N	97°22′56.6″ W	05/24/2019	Subfossil	≈ +3	LP	Ara
ATX-C2	19°20′12.5″ N	97°26′55.9″ W	05/23/2019	Subfossil	≈ +1.2	ATX	Ara
ATX-C3	19°20′12.5″ N	97°26′55.9″ W	05/23/2019	Subfossil	≈ +2.2	ATX	Ara
ATX-C5	19°20′12.5″ N	97°26′55.9″ W	05/23/2019	Subfossil	≈ +3.7	ATX	Ara
ATX-C6	19°20′12.5″ N	97°26′55.9″ W	05/23/2019	Subfossil	≈ +4.7	ATX	Ara
ATX-C7	19°20′12.5″ N	97°26′55.9″ W	05/23/2019	Subfossil	≈ +4.9	ATX	Ara
ATX-C8	19°20′12.5″ N	97°26′55.9″ W	05/23/2019	Subfossil	≈ +5.2	ATX	Ara
ATX-C9	19°20′12.5″ N	97°26′55.9″ W	05/23/2019	Subfossil	≈ +6	ATX	Ara
ATX19-mb-5m	19°19′55″ N	97°27′05″ W	05/23/2019	Underwater (oxic)	−5	ATX	Ara
ATX19-mb-10m	19°19′55″ N	97°27′05″ W	05/23/2019	Underwater (oxic)	−10	ATX	Ara
ATX19-mb-15m-a	19°19′55″ N	97°27′05″ W	05/23/2019	Underwater (mostly oxic?)	−15	ATX	Ara
ATX19-mb-20m	19°19′55″ N	97°27′05″ W	05/23/2019	Underwater (oxic to anoxic)	−20	ATX	Ara

(Continues)

TABLE 2 | (Continued)

Sample name	Latitude	Longitude	Sampling date	Underwater // Subfossil (oxygen conditions)	Depth/height relative to current water level (m)	Facies group	Main carbonate mineralogy
Albesp2014-01	19°54′27.4″ N	101°46′1.1″ W	5/15/2014	Underwater (oxic)	−0.5	Albesp	Cal, MHC
Albesp2019 (fossile)	19°54′27.8” N	101°46′1.0″ W	5/29/2019	Subfossil	≈ +0.3	Albesp	Cal, MHC

Note: Albesp2014-01 was first described by Zeyen et al. (2019).
Abbreviations: AL, Alchichica; Albesp, Alberca de los Espinos; Ara, aragonite; ATX, Atexcac; Cal, calcite; Hmg, hydromagnesite; LP/PR, La Preciosa; MHC, monohydrocalcite.

Dijon). Measurements were achieved under a 20-mbar vacuum, using an x-ray excitation energy of 50 kV and a current of 270 μA. Elemental maps were up to 2000 × 1500 pixels and were acquired over up to 4.5 h with a dwell time of 10 ms per pixel.

3.4 | Elemental and Isotopic Analyses

3.4.1 | Major and Minor Element Contents of Rock Samples

Concentrations of major and trace elements from ground microbialite powders were measured at the Service d'Analyse des Roches et Minéraux (SARM, Centre de Recherches Pétrographiques et Géochimiques, Nancy, France) using inductively coupled plasma (ICP-) atomic emission spectroscopy (AES) and mass spectrometry (MS). ICP-AES and ICP-MS were performed using an ICap 6500 and an iCapQ (Thermo Fisher), respectively, after alkali fusion of rock samples with $LiBO_2$ (sample to $LiBO_2$ flux ratio of 1:3) followed by dissolution in HNO_3. About 2 g of sample were used for these analyses. The uncertainties on element quantification were between 1% and 25% depending on their concentrations and were assessed from relative standard deviations calculated on a minimum of 100 measurements of reference geochemical standards used for calibration (BR (basalt), AN-G (anorthosite), UB-B (serpentinite), DR-N (diorite), and GH (granite) provided by the SARM).

3.4.2 | Bulk Carbonate Contents, C and O Isotope Compositions, and Micro-Drill Analyses

The total carbonate contents of microbialites were initially determined by weighing samples before and after decarbonation with 1 N HCl overnight. Carbonate carbon and oxygen isotopic compositions ($\delta^{13}C_{carb}$, $\delta^{18}O_{carb}$) were carried out on bulk and micro-drilled powdered microbialites at the GISMO platform (Dijon). Micro-drill powders were sampled with a micro-dremel, allowing a sampling diameter of about 1 mm. Sample aliquots (70–140 μg) were loaded in glass vials and analyzed using a Kiel IV carbonate preparation device coupled with a ThermoScientific Delta V Plus IRMS. The preparation device transforms the carbonates into CO_2 by acidification with a few drops of H_3PO_4 at a controlled temperature (~70°C), purifies the CO_2 with an adjustable temperature liquid nitrogen trap and concentrates it in a micro-volume before sending it to the mass-spectrometer. Three samples were analyzed for bulk $\delta^{13}C_{carb}$ and $\delta^{18}O_{carb}$ using a ThermoScientific Delta Ray infrared mass-spectrometer (GISMO platform, Dijon). About 3 mg of powders were loaded in Exetainer tubes, subsequently flushed with He gas and acidified with a dozen drops of ≥ 100% H_3PO_4, reacting for more than 12 h at ~20°C before measurement.

Both $\delta^{13}C_{carb}$ and $\delta^{18}O_{carb}$ are reported relative to the international standard VPDB scale. NBS-19 certified material was used for calibration ($\delta^{13}C = +1.95‰$, $\delta^{18}O = +2.20‰$). Instrumental drift was accounted for based on NBS-19 measured each 20 samples. Linearity of the mass-spectrometer was monitored between each measurement sequence. Moreover, similar volumes of CO_2 for the standards and samples were injected in the mass-spectrometer to avoid linearity issues. This was achieved by automatic adjustment of the variable volume chambers in the Kiel IV device, and by weighing similar CO_2-equivalent amounts of powder between samples and standards (differing from less than 10% on average). Reproducibility was better than 0.1‰ and 0.2‰ for $\delta^{13}C$ and $\delta^{18}O$, respectively, when measured with the Delta V Plus, and better than 0.2 and 0.4‰ when using the Delta Ray. Out of the 34 samples measured for C and O isotopes of bulk carbonates, 29 were at least duplicated and showed average external reproducibility of ±0.2 and ± 0.3‰, respectively. For samples that were not duplicated, the error bars on graphics correspond to the standards' reproducibility from the same sequence of measurements. The acid-carbonate oxygen isotope fractionations associated with the acid digestion of carbonates were corrected according to mineralogy using α_{CO2}(ACID)-carbonate values of 1.0087, 1.0091, and 1.0101 at a temperature of 71°C (1.0105, 1.0108, and 1.0123 at 20°C) for calcite, aragonite, and hydromagnesite, respectively (Kim et al. 2015 and references therein). The weighted averages were calculated considering the specific carbonate mineralogy of each microbialite sample and assuming that the unknown α_{CO2}(ACID)-carbonate of hydromagnesite corresponds to that of magnesite.

3.4.3 | Total Organic C Content and Isotope Composition

Total organic carbon (TOC) contents and isotope compositions were measured on carbonate-free residues of the microbialite powders, produced after overnight 1 N HCl digestion. Aliquots of dried carbonate-free samples (~ 2–70 mg) were weighed in tin capsules. The TOC content and $\delta^{13}C_{TOC}$ values were determined at the GISMO platform (Dijon) using a Vario MICRO cube elemental analyzer (Elementar GmbH, Hanau, Germany) coupled in continuous flow mode with an IsoPrime IRMS (Isoprime, Manchester, UK). USGS 40 certified material was used for calibration and had a reproducibility better than 0.1‰ for $\delta^{13}C_{TOC}$. Sample analyses were at least duplicated and showed average external reproducibility of 0.1‰ for $\delta^{13}C$. External reproducibility for TOC content was 0.1 wt. % on average. $\delta^{13}C_{TOC}$ are reported on the VPDB scale.

3.4.4 | Major Element Concentrations in Water Samples

Dissolved concentrations of major elements were measured on acidified lake waters (2% HNO_3^-) at the Pôle Spectrométrie Océan (Plouzané, France) by ICP-AES (Horiba Jobin). Dissolved sulfate (SO_4^{2-}) and chloride (Cl^-) concentrations were determined by ion-chromatography with conductivity detection (ICS-1100, Thermo Scientific Dionex) at the Institut de Physique du Globe de Paris (IPGP, France). Concentrations were calibrated based on multi-elemental standard solutions prepared in the lab (initial standard solutions from SCP science and Chemlab). The reproducibility for cation and anion concentration measurements based on these standard solutions was better than 5%.

3.4.5 | Dissolved Inorganic C and H_2O Isotopic Analyses

The data and acquisition method for DIC concentrations and isotope compositions of the lake waters can be found in Havas et al. (2023a). They were measured following the protocol described in Assayag et al. (2006). The reproducibility for samples $\delta^{13}C_{DIC}$ was better than 0.2‰ (Havas et al. 2023a). The [DIC], $\delta^{13}C_{DIC}$, and $\delta^{18}O_{H_2O}$ of groundwater samples were analyzed by the Beta Analytic laboratory, via a protocol similar to Assayag et al. (2006) for DIC, and by Cavity Ring-Down Spectroscopy (CRDS) for H_2O analyses. The $\delta^{13}C_{DIC}$ and $\delta^{18}O_{H_2O}$ are reported relative to the international standard VPDB and VSMOW scale, respectively. The reproducibility for both in-house standards and samples measurement was better than 0.1 and 0.2‰ for $\delta^{13}C_{DIC}$ and $\delta^{18}O_{H_2O}$, respectively.

3.5 | Geochemical Calculations

In order to evaluate whether the microbialite carbonates precipitated in isotopic equilibrium with their respective lake waters, we determined the offset between measured DIC and H_2O isotope signals and (calculated) isotope compositions of the fluid in equilibrium with the microbialite carbonates such that:

$$\Delta^{13}C_{DIC-eq} = \delta^{13}C_{DIC-eq} - \delta^{13}C_{DIC-measured} \quad (1)$$

and,

$$\Delta^{18}O_{H_2O-eq} = \delta^{18}O_{H_2O-eq} - \delta^{18}O_{H_2O-measured} \quad (2)$$

The isotope compositions of the "equilibrium fluid" depend on the temperature-dependent equilibrium isotopic fractionations between the bulk solid carbonates and DIC for C ($\Delta^{13}C_{carb\text{-}DIC}$), and H_2O for O ($\Delta^{18}O_{carb\text{-}HO}$) following the equations:

$$\delta^{13}C_{DIC-eq} = \delta^{13}C_{carb} - \Delta^{13}C_{carb-DIC} \quad (3)$$

and,

$$\delta^{18}O_{H_2O\text{-}eq}\delta^{18}O_{carb} - \Delta^{18}O_{carb-H_2O} \quad (4)$$

where $\delta^{13}C_{carb}$ and $\delta^{18}O_{carb}$ are the bulk C and O isotope compositions of microbialite carbonates. Since Mexican microbialites contain a mix of several carbonate phases, the $\Delta^{13}C_{carb\text{-}DIC}$ and $\Delta^{18}O_{carb\text{-}HO}$ parameters represent a weighted average of the fractionations induced by the precipitation of these different carbonate phases such that:

$$\Delta^{13}C_{carb-DIC} = \Sigma\, \Delta^{13}C_{i\_carb-DIC}{}^{*}\, f_i \quad (5)$$

and,

$$\Delta^{18}O_{carb-H_2O} = \Sigma\, \Delta^{18}O_{i\_carb-H_2O}{}^{*}\, f_i \quad (6)$$

where f_i represents the relative proportions of each carbonate phase as determined by XRD. Whereas oxygen isotope fractionations in the literature are reported directly between solid carbonates and H_2O, carbon isotope fractionations are expressed relative to specific DIC species—which vary according to pH. Their respective isotopic compositions (e.g., $\delta^{13}C_{CO_3^{2-}}$) thus need to be determined, based on the measured $\delta^{13}C_{DIC}$, the fractionation factors ε, and the concentration of each DIC species (Zeebe and Wolf-Gladrow 2001). In the case of CO_3^{2-} for example:

$$\delta^{13}C_{CO_3} = \left([DIC] * \delta^{13}C_{DIC} - \left([CO_2]_{(aq)}{}^{*}\varepsilon_{CO_2aq-CO_3} + [HCO_3] * \varepsilon_{HCO_3-CO_3}\right)\right) / \left([CO_2]_{(aq)}{}^{*}(1+\varepsilon_{CO_2aq-CO_3}/1000) + [HCO_3] * (1+\varepsilon_{HCO_3-CO_3}/1000) + [CO_3]\right) \quad (7)$$

The concentrations of the different DIC species were computed with PHREEQC based on measurements of pH and total [DIC] from Havas et al. (2023a), as well as major ions concentrations (Table S2). The equations and references used in the calculation of ε parameters, as well as $\Delta^{13}C_{i\_carb\text{-}DIC}$ and $\Delta^{18}O_{i\_carb\text{-}HO}$ parameters are summarized in Table S3. Because C isotopes equilibrate quickly among the different DIC species (e.g., within about 30 s at pH = 8.3; Zeebe 1999), we consider that the carbonate precipitates are in isotopic equilibrium with all DIC species. The equilibrium C isotope fractionation can thus be calculated between the microbialites carbonate and any of the DIC species (e.g., $\Delta^{13}C_{i\_carb\text{-}CO3}$), and then be reported against the total "equilibrium" $\delta^{13}C_{DIC\text{-}eq}$ following the equation:

$$\delta^{13}C_{DIC-eq} = \delta^{13}C_{carb} - \Sigma\left(\Delta^{13}C_{i\_carb-CO_3}{}^{*}f_i\right) - \Delta^{13}C_{CO_3-DIC} \quad (8)$$

Finally, this result can be compared with $\delta^{13}C_{DIC\text{-}measured}$ (Equation 1). The measured $\delta^{13}C_{DIC}$ and $\delta^{18}O_{H_2O}$ values used in Equations (1) and (2), respectively, were measured at different depths in the four lakes and are described in the result Section 4.5 (Table S2).

There is no specific data available in the literature about C isotope fractionation for hydromagnesite precipitation ($Mg_5(CO_3)_4(OH)_2·4H_2O$), but only for dypingite ($Mg_5(CO_3)_4(OH)_2·5H_2O$) (Harrison et al. 2021) and magnesite ($MgCO_3$) (Aharon 1988). Converted to the same conditions, the isotopic fractionations for the two latter phases are very similar (within ~0.2‰). Therefore, we calculated $\Delta^{13}C_{hydromagnesite\text{-}DIC}$ using results by Aharon (1988) on magnesite since a temperature-dependent relationship is provided by the author, but corrected it by 0.2‰ as dypingite's chemical composition is closer to that of hydromagnesite (Table S3). We assume that the fractionations induced by Mg-calcite and monohydrocalcite precipitation (only found in Alberca) are equal to that of calcite (Table S3).

For the calculation of isotopic fractionations, we estimate the average temperatures of microbialites formation based on temperature depth profiles from May 2019 in the four lakes (Havas et al. 2023a), and temperature monitoring in the entire water column of Alchichica between 2003 and 2016 (Macek et al. 2020). For surface microbialites, we use an average temperature of 18°C for the SOB lakes (Alcocer et al. 2022), and 20°C for Lake Alberca. Average temperatures of 16.5°C are used at 20 m depth (Table S2 and Havas et al. 2023a). Note that temperatures influence the O isotope fractionations induced by carbonate precipitation by ~0.2‰/°C, but have a negligible effect on the calculated $\delta^{13}C_{DIC\text{-}eq}$ (Figure S2).

4 | Results

4.1 | Mineralogical Composition and Total Organic Carbon Contents

The bulk mineralogy of microbialites is consistent with previous characterizations by Zeyen et al. (2021). Carbonates represent the main family of mineral phases with a bulk content of 82.7 ± 3.2 wt. % in Alberca ($n = 2$), 82 ± 4 wt. % in La Preciosa ($n = 4$), 89 ± 7 wt. % in Atexcac ($n = 11$), 96.3 ± 0.4 and 98 ± 2 wt. % in the "brown" and "white" facies from Alchichica ($n = 6$ and 14), respectively (Table S1). Rietveld refinement after XRD analyses provides the proportion of each crystalline phase relative to the bulk crystalline phases (Table S1). Alberca microbialites consist mostly of Mg-calcite ($[Mg_{\leq 0.1}Ca_{\geq 0.9}]CO_3$) and monohydrocalcite ($CaCO_3·H_2O$), which represent about 85% and 12% of the crystalline phases, respectively (Table S1). Aragonite ($CaCO_3$) is the main phase of La Preciosa and Atexcac microbialites, representing 99.5 ± 0.9 and 97 ± 3% of their respective crystalline assemblage (Table S1). In Alchichica, the brown microbialites consist mostly of aragonite (97 ± 1%), whereas the white microbialites consist mainly of hydromagnesite ($Mg_5(CO_3)_4(OH)_2·4H_2O$; 86 ± 7%) and aragonite (14 ± 7%).

In Alberca, La Preciosa, and Atexcac, broad XRD peaks at 19°–20°, 34°–36°, and 61° (2θ) also show the presence of an abundant poorly-crystalline Mg-silicate phase not considered in the above-mentioned Rietveld analysis (Figure 3), which likely corresponds to authigenic kerolite ($Mg_3Si_4O_{10}(OH)_2.H_2O$), as determined by Zeyen et al. (2015). By considering that it represents the only phase after subtracting the carbonates, TOC, and other minor crystalline phases, we calculate that kerolite represents on average 15 ± 2, 16 ± 4, and 8 ± 6 wt. % in microbialites from Alberca, La Preciosa, and Atexcac, respectively (Table S1). Other authigenic phases are also found in several microbialites as minor phases, including Fe-bearing layered double hydroxides (LDH) previously described by Zeyen et al. (2019, 2021). Detrital phases such as quartz and feldspars can be found as well (mostly < 2%; up to 6% for ATX-C2) (Table S1).

The TOC content of microbialites averaged 2.0 ± 0.6 wt. % in Alberca, 1.7 ± 0.2 wt. % in La Preciosa, 1.1 ± 0.5 wt. % in Atexcac, and 0.6 ± 0.2 wt. % and 0.4 ± 0.2 wt. % in Alchichica brown and white microbialites, respectively (Table S1).

4.2 | Petrographic Descriptions

La Preciosa microbialites are characterized by: (i) widespread and poorly-structured microbial mats permineralized by aragonite and Mg-silicates, and (ii) important fracturing and secondary infilling of cavities with carbonated muds and cements, detrital and microbialite grains, sometimes covered again by micrometric needle-shaped cements (Figure 4a–c). The µXRF chemical mapping shows that the grains are rich in Fe and/or Si and Mg, or Ca, thus either produced by the erosion of volcanic rocks (typically rich in Fe and Si) or corresponding to microbial carbonates (rich in Ca) and Mg-silicate phases (rich in Mg and Si) eroded from the surrounding microbialites (Figure 5g). Remnants of filamentous and coccoidal organisms are common in the permineralized biofilms, sometimes interspersed with isopachous carbonate cements (Figure 4b,c), and frequently associated with ostracod and gastropods shells.

Atexcac microbialites appear poorly organized and highly fractured under visible light microscopy, forming dark and isopachous patches. The fractures can be filled by early light-colored cements, muds, and/or detrital grains from the surrounding microbialite matrix. Abundant diatoms were found, together with coccoidal and filamentous bacteria (Figure 4e,f). Several samples (ATX19-20 m, ATX-C2 and -C3) harbor an additional fabric which suggests possible emersion periods. This fabric is mostly circular-shaped or speleothem-like, but can be found as flat laminae (Figure S3); it appears as pending and in-filling cavities, usually growing on past permineralized microbialites. It can be covered by detrital particles and mud, or by a subsequent microbial biofilm (Figure S3). The highest samples on the microbialite transect sampled in Atexcac (located from 8 to 11 m above the lake level), which appeared more eroded and altered, and one submerged sample showed clearly distinguishable botryoidal fabrics under visible light in thin sections (Figure S4), suggestive of intense recrystallization through early diagenesis. They were excluded from the present study.

In Alchichica white microbialites, hydromagnesite appears as massive and structure-less patches under visible light microscopy, whereas aragonite concentrates near the edges and bordering cavities (Figure 4g,h,i). Peloidal hydromagnesite particles sometimes agglutinate and incorporate the hydromagnesite matrix by a cementation process (Figure 4g,j). In these samples, organic-rich layers, highlighted by high UV-epifluorescence, are associated with aragonite in the outer parts

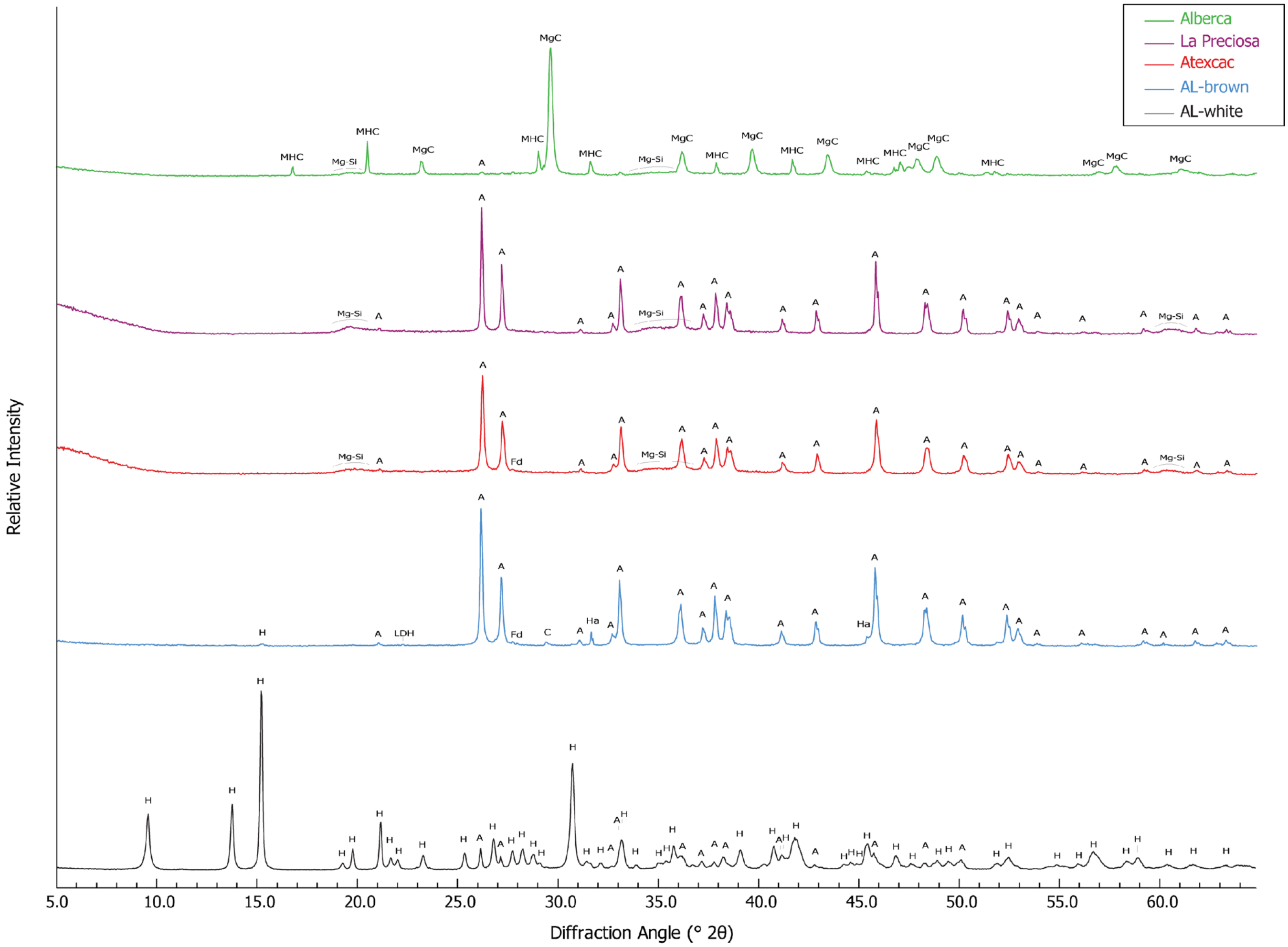

FIGURE 3 | Powder x-ray diffraction (XRD) patterns of microbialite samples from Alberca de los Espinos (green, 'Albesp2014-01'), La Preciosa (purple, 'PR-3'), Atexcac (red, 'ATX19-20m'), Alchichica "brown" (blue, 'AL-T-9') and "white" (black, 'AL-R-3') microbialites. The main phases detected are monohydrocalcite (MHC), Mg-calcite (MgC), poorly-crystalline Mg-silicates (Mg-Si), aragonite (A), feldspar (Fd), hydromagnesite (H), layered double hydroxide (LDH), calcite (C), halite (Ha). Peaks of phases including 'LDH' and 'Mg-Si' appear flatten in the above representation but clearly stand out when single diffraction patterns are visualized.

of the microbialites (Figure 4i). Biological remnants are rare in the "white microbialites".

Brown microbialites mineral matrix is less massive than in white microbialites. It consists of detrital grains trapped and bound by microbial biofilms and/or mineralized biofilms, which, on the contrary to what is seen in white microbialites, are ubiquitous (Figure 4n,o). Part of the porosity consists of holes left by the former presence of insect nests and/or small plant roots or algae (Figure 4k,l,m), which are also visible at a macroscopic scale sometimes. Additionally, the brown microbialites are characterized by pervasive traces of grazing organisms and heterotrophic bacteria. For example, numerous fragments of ostracod and gastropod shells were found, as well as pyrite framboids contiguous to the biofilms (Figure 4k,l,m).

Finally, petrographic observations of Alberca microbialites were thoroughly carried out in a past study and show dense clusters of filamentous microfossils encrusted in both Mg-calcite and Mg-silicate phases (Zeyen et al. 2021).

4.3 | Elemental Geochemistry

Calcium (Ca averages 21.5 ± 11.5 wt. %), magnesium (Mg averages 8.4 ± 8.4 wt. %), and silicon (Si averages 3.1 ± 4.1 wt. %) are the most abundant elements in the studied microbialites (Table S4). A ternary diagram showing Ca-Mg-Si relative abundances highlights the different mineralogical compositions found in the microbialites of the four lakes (Figure 5a). As shown by Zeyen et al. (2021), the white microbialites from Alchichica follow a line between Mg and Ca endmembers reflecting the relative contents of hydromagnesite and aragonite (Figure 5a), with very low concentration of Si, except for samples slightly contaminated with detrital grains. Alchichica brown microbialites (all) plot in the Ca corner, being almost entirely composed of aragonite. Along with these samples, microbialites from the other three lakes plot on a line between the Ca endmember and a Mg-Si mixture in stoichiometric proportions close to that of the poorly crystalline Mg-silicate phases kerolite and stevensite (Zeyen et al. 2021). All microbialites sampled show positive Eu anomalies (Eu* measured as Eu/[0.66Sm + 0.33 Tb]) with the

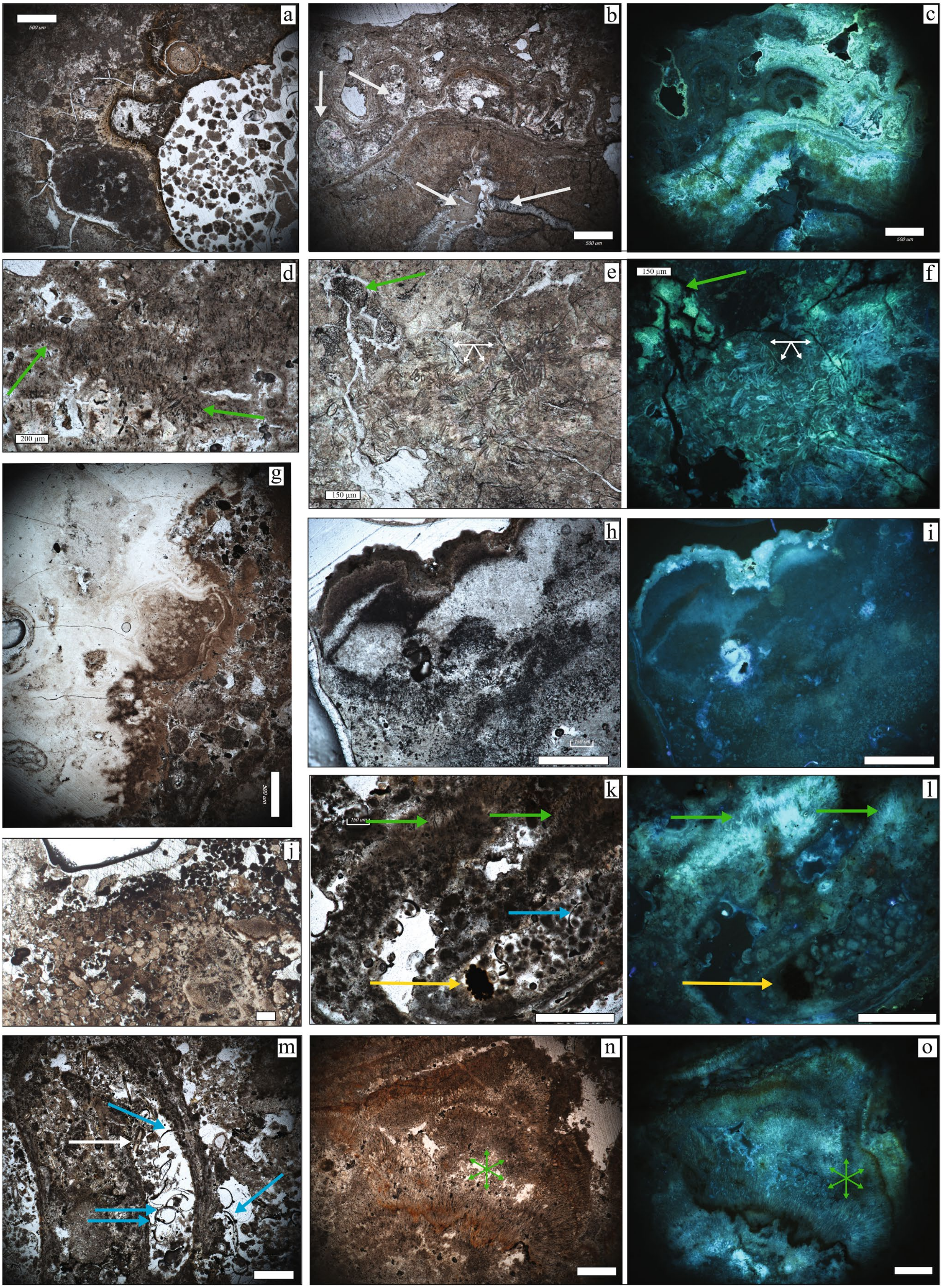

FIGURE 4 | Legend on next page.

FIGURE 4 | Plane-polarized light and UV-epifluorescence photographs of the Mexican. (a–c) La Preciosa thin sections ('PR-3' and 'LP-50cm'). (d–f) Atexcac thin sections ('ATX-C8' and 'ATX19-20m'). Photographs in (g) ('AL-R-4'), (h, i) ('AL19-5m'), and (j) ('AL-R-3') are all from the "white" facies in Alchichica, (k–m) ('AL-T-5'), and (n, o) ('AL-T-9') from the "brown" facies in Alchichica. Gray arrows in La Preciosa photographs point out fracture-filling muds and secondary cements; green arrows point out the filamentous and coccoidal bacteria; white arrows point out diatoms; blue arrows point out ostracod shells, and yellow arrows pyrite grains. White scale bars represent 500 μm unless noted.

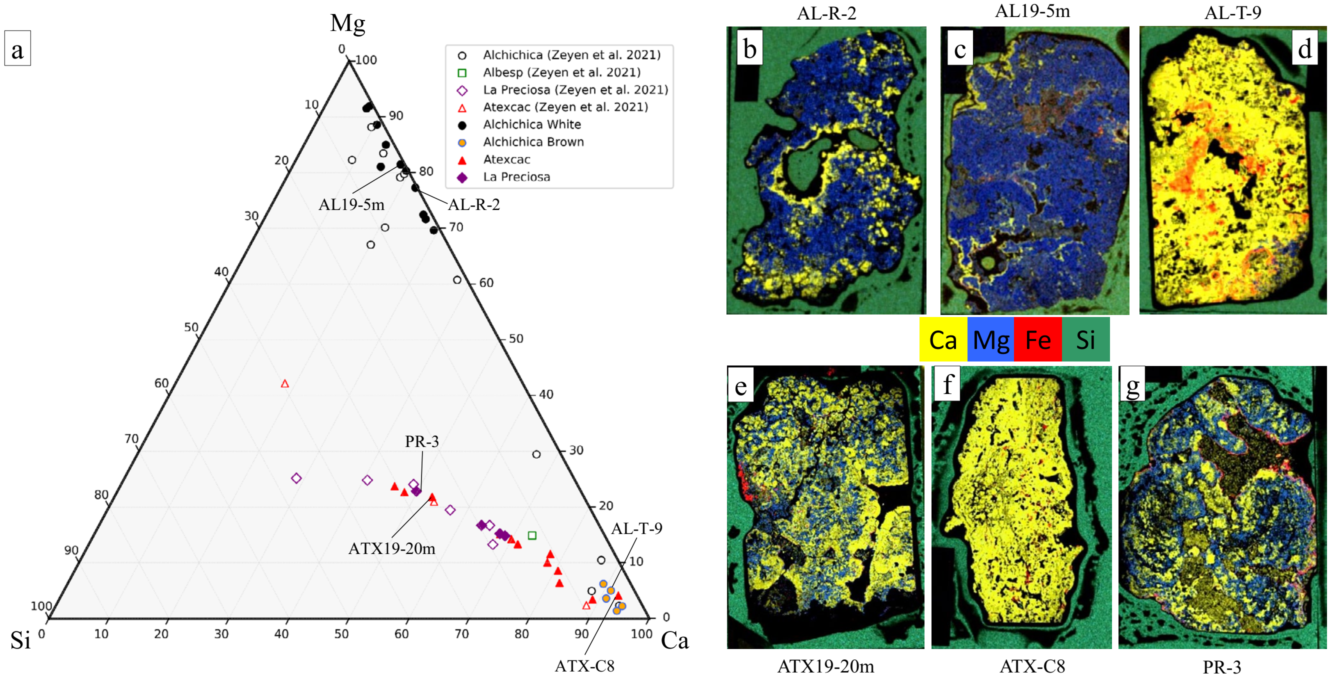

FIGURE 5 | Major element geochemistry of the Mexican microbialites. (a) Ternary diagram reporting the microbialites bulk relative abundances of Mg, Ca, and Si normalized to the sum of the three elements (as molar ratios). Empty dots correspond to data from Zeyen et al. (2021) study. (b-g) X-ray fluorescence (XRF) chemical maps of microbialites from Alchichica (b-d), Atexcac (e-f), and La Preciosa (g), where calcium, magnesium, iron, and silicon relative abundances are represented in yellow, blue, red, and green, respectively.

highest recorded anomaly found in Alchichica brown microbialites (2 on average, vs. 1.5 in the other lakes; Table S4). Alchichica brown microbialites also show Fe contents higher than in any other sample (Table S4; 1.4 vs. 0.3 wt. % on average).

The thin section μXRF maps are consistent with petrographic observations and microbialites mineralogy and bulk chemistry (Figure 5). In Alchichica white microbialites, a Ca-rich phase (i.e., aragonite) concentrates near the edges and in the fractures (Figure 5b,c). Brown microbialites appear more porous, with a mineral matrix dominated by Ca (aragonite) and abundant dispersed Fe contained in Fe-bearing LDH (Figure 5d). By contrast, Si is abundant in Atexcac and La Preciosa thin sections, and is associated with Mg, supporting the presence of Mg-silicate phases (Figure 5e–g; Figure S5).

4.4 | Carbonate and Organic C Isotope Compositions

In Alberca microbialites, the bulk carbonate C and O isotope compositions ($\delta^{13}C_{carb}$ and $\delta^{18}O_{carb}$) average 0.8 ± 0.2 and −0.1 ± 0.8‰, respectively (Figure 6a.) The calculated $\delta^{13}C_{DIC\text{-}eq}$ and $\delta^{18}O_{H_2O\text{-}eq}$ (DIC and water O isotope compositions in equilibrium with the bulk carbonates) average − 0.5 ± 0.2‰ and 1.6 ± 0.8‰, respectively (Figure 6b). The bulk organic C isotope compositions ($\delta^{13}C_{org}$) average − 20.8 ± 2.5‰ (Table S5).

In La Preciosa, the microbialites $\delta^{13}C_{carb}$ and $\delta^{18}O_{carb}$ average 4.0 ± 0.5 and − 1.6 ± 0.1‰, respectively, corresponding to a $\delta^{13}C_{DIC\text{-}eq}$ of 1.1 ± 0.5‰ and a $\delta^{18}O_{H_2O\text{-}eq}$ of −1.0 ± 0.2‰ (Figure 6). The $\delta^{13}C_{org}$ average − 23.5 ± 1.4‰ (Table S5). The $\delta^{13}C_{carb}$ and $\delta^{18}O_{carb}$ determined from micro-drilling in microbialite 'PR-2' ranged from 1.5 to 4.9 and from −2.6‰ to −0.6‰, respectively, corresponding to $\delta^{13}C_{DIC\text{-}eq}$ from −1.5‰ to 1.9‰ and $\delta^{18}O_{H_2O\text{-}eq}$ from −2.8‰ to 0.8‰ (Figure 7).

In Atexcac, the microbialites $\delta^{13}C_{carb}$ and $\delta^{18}O_{carb}$ average 3.2 ± 0.8 and −0.7 ± 0.9‰, respectively, both parameters correlating well ($R^2 = 0.88$; Figure 6). The trend recorded by $\delta^{13}C_{DIC\text{-}eq}$ and $\delta^{18}O_{H_2O\text{-}eq}$ is almost identical to that between $\delta^{13}C_{carb}$ and $\delta^{18}O_{carb}$. The $\delta^{13}C_{DIC\text{-}eq}$ averages 0.3 ± 0.8‰, and $\delta^{18}O_{H_2O\text{-}eq}$ averages −0.1 ± 0.9‰. The $\delta^{13}C_{org}$ average − 27.4 ± 0.6‰ (Table S5).

The Alchichica brown microbialites $\delta^{13}C_{carb}$ and $\delta^{18}O_{carb}$ average 2.2 ± 0.3 and −2.3 ± 0.5‰. Corresponding $\delta^{13}C_{DIC\text{-}eq}$ and $\delta^{18}O_{H_2O\text{-}eq}$ average − 0.8 ± 0.3‰ and −1.8 ± 0.6‰, respectively (Figure 6). Brown microbialites $\delta^{13}C_{org}$ average − 25.2 ± 1.0‰ (Table S5). The Alchichica white microbialites $\delta^{13}C_{carb}$ and $\delta^{18}O_{carb}$ average

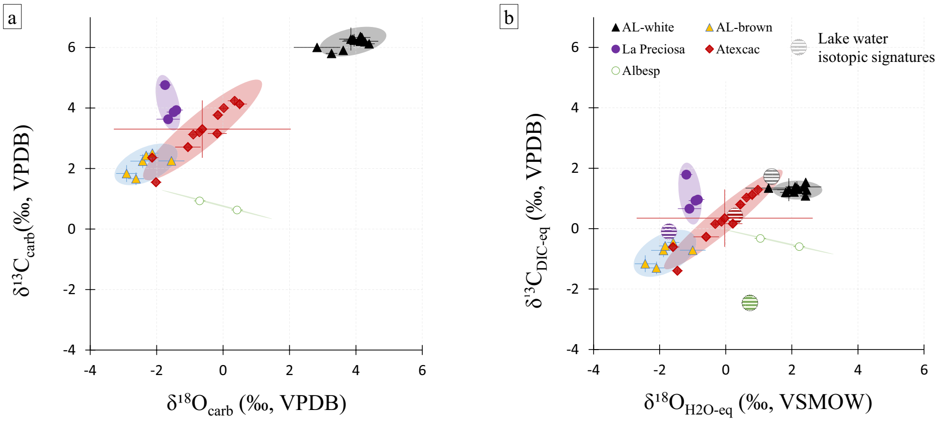

FIGURE 6 | Microbialite bulk carbonate carbon and oxygen isotope compositions (a) and recalculated dissolved inorganic carbon (DIC) and water oxygen isotope compositions in equilibrium with the microbialites (b). Each lake water DIC and H_2O isotopic signatures are represented in (b) by the small transparent circles in green for Alberca, purple for La Preciosa, red for Atexcac and blue for Alchichica. Error bars correspond to standard deviations from a minimum of two replicate analyses. Ellipses represent 95% confidence ellipses.

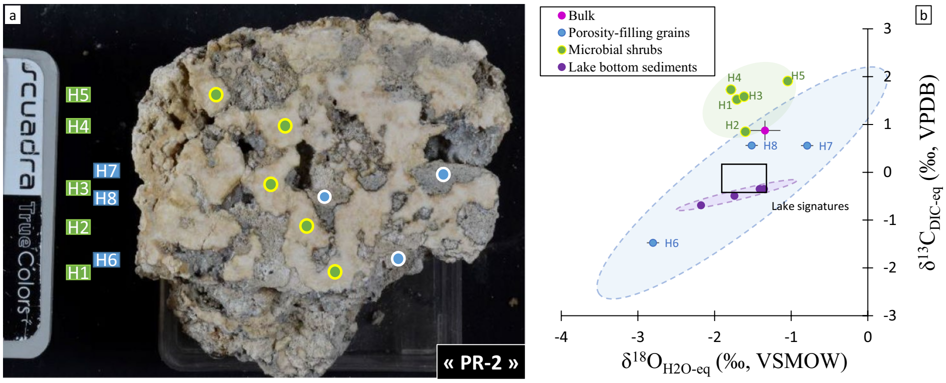

FIGURE 7 | Micro-drill results for the “PR-2” microbialite from Lake La Preciosa. (a) Photograph of the sample and location of micro-drilling in the microbial shrubs (in green) and void-filling sediments (in blue). (b) Carbon and oxygen isotope compositions of DIC and H_2O in equilibrium ($\delta^{13}C_{DIC\text{-}eq}$ and $\delta^{18}O_{H_2O\text{-}eq}$) with the micro-drilled and bulk microbialite carbonates, as well as of the bottom lake sediments (purple). The black rectangle represents the water isotopic signature of Lake La Preciosa. Ellipses represent 95% confidence ellipses.

6.2 ± 0.2 and 3.9 ± 0.5‰, respectively. Corresponding $\delta^{13}C_{DIC\text{-}eq}$ and $\delta^{18}O_{H_2O\text{-}eq}$ average 1.3 ± 0.1‰ and 3.5 ± 0.3‰, respectively (Figure 6). Their $\delta^{13}C_{org}$ average −25.0 ± 1.1‰ (Table S5).

4.5 | Geochemical Characteristics of the Lake and Ground Waters

Total DIC isotope compositions were measured at different depths in the four stratified water columns and in two different years (May 2019 and October 2022) except in Alberca which was only sampled in May 2019 (Havas et al. 2023a). The $\delta^{13}C_{DIC}$ of lake waters show small variations between the different depths and years of sampling (mostly ≤ 0.6‰; Table S2). The reference $\delta^{13}C_{DIC}$ values used in the calculations of $\Delta^{13}C_{DIC\text{-}eq}$ are those of May 2019, when most microbialites were sampled. For shallow and emerged microbialites, the $\delta^{13}C_{DIC}$ of surface waters (< 5 m) were used as reference and are equal to −2.6‰, 0.1‰, 0.4‰, and 1.9‰ in Alberca, La Preciosa, Atexcac, and Alchichica, respectively (Table S2). For deeper microbialites (in Atexcac and Alchichica), the reference $\delta^{13}C_{DIC}$ were chosen from the same depths at which microbialites were collected (Table S2).

The analysis of oxygen isotope compositions from the 2022 surface waters of La Preciosa, Atexcac, and Alchichica provides $\delta^{18}O_{H_2O}$ values of −1.9‰, 0.4‰, and 1.6‰, respectively, and were used as reference values in the calculation of $\Delta^{18}O_{H_2O\text{-}eq}$ (Table S2). Also measured in 2019 in Alchichica at a depth of 35 m, $\delta^{18}O_{H_2O}$ equaled to 1.2‰, close to the value measured in 2022 at the same depth (0.9‰; Table S2), suggesting stable $\delta^{18}O_{H_2O}$ values in the recent years. The $\delta^{18}O_{H_2O}$ also shows relatively small variations with depth in these lakes (< 0.6‰; Table S2). The $\delta^{18}O_{H_2O}$ were not measured in Alberca de los Espinos. Assuming that the surficial sediment carbonates at the bottom of the lake precipitate in equilibrium with waters in the upper part of Lake Alberca (Havas et al. 2023a), we calculated the water O isotope composition in equilibrium with these carbonates, resulting in a $\delta^{18}O_{H_2O}$ of 0.8‰.

Three samples from the groundwater flowing toward lake Alchichica were analyzed and their DIC concentrations ranged from 6.4 to 11.7 mM, $\delta^{13}C_{DIC}$ from −5.1‰ to −2.7‰, and $\delta^{18}O_{H_2O}$ from −12.8‰ to −7‰ (Figure 8; Table S2). These solutions are characterized by aragonite saturation indexes (SI_{ara}) varying between 0.5 and 1.0, SI_{HMg} (with respect to hydromagnesite) between ~ −9 and −6, and dissolved Mg/Ca molar ratios between 1 and 2

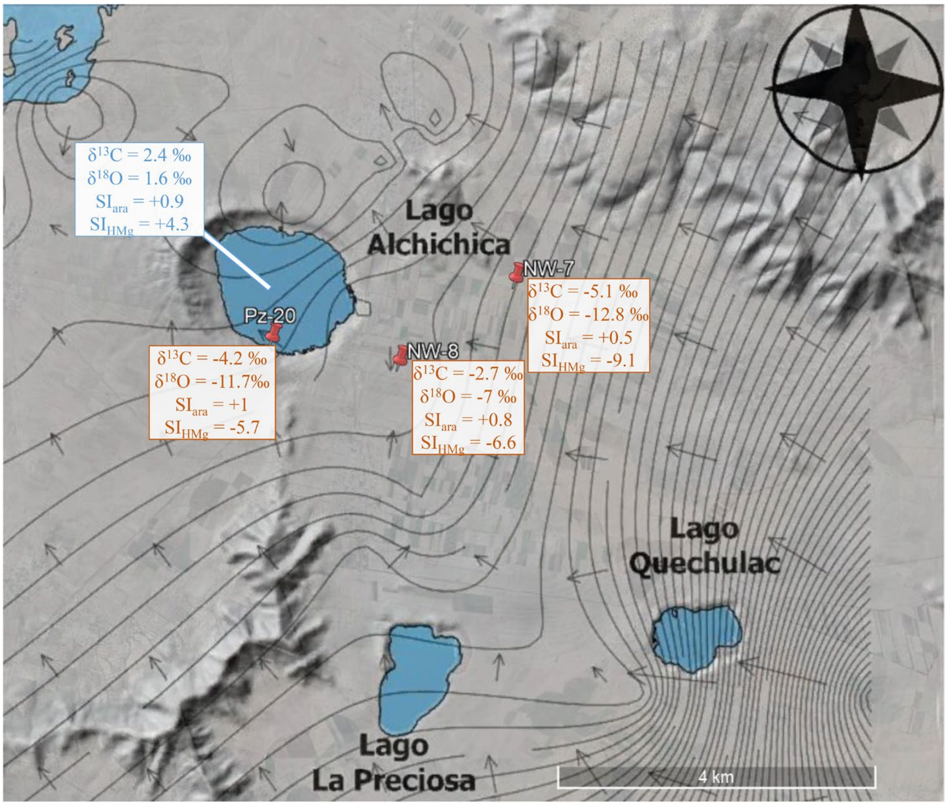

FIGURE 8 | Hydrological map of the Serdán-Oriental Basin showing the main direction of the groundwater flow in the aquifer "de Libres Oriental" together with some results of the aqueous geochemistry analyses. The map is from Silva Aguilera (2019) and is zoomed on the area of Alchichica and La Preciosa lakes. Isotopic compositions of the DIC ($\delta^{13}C$), water oxygen ($\delta^{18}O$), and saturation indexes for aragonite and hydromagnesite (SI_{ara} and SI_{HMg}) are shown in orange boxes for three of the wells preceding Alchichica. The same data for Alchichica surface water sampled at the same time as the well waters (October 2022) is shown for comparison in the blue box. The $\delta^{13}C$ and $\delta^{18}O$ are expressed in ‰ relative to VPDB and VSMOW, respectively.

(Figure 8; Table S2). By contrast, lake waters SI_{ara} vary between 0.6 and 1.4, and SI_{HMg} between −0.25 and 4.3 (see details in Table S2).

5 | Discussion

5.1 | Organic C Isotope Signatures and Microbial Community Compositions

Bulk organic C isotope signatures suggest a primary photosynthetic origin of the microbialites biomass in the four lakes. In La Preciosa, Atexcac, and Alchichica, $\Delta^{13}C_{org\text{-}DICeq}$ average −25‰, −28‰ and −26‰, respectively (Figure S6). Comparable signatures were similarly interpreted in Pavilion Lake (−26.8‰; Brady et al. 2010), in Cuatro Ciénagas (−30‰ to −31‰; Breitbart et al. 2009), and Kelly Lake (−26‰ to −29‰; White III et al. 2020). In Alberca, the bulk organic C isotope signals are significantly ^{13}C-depleted, with $\Delta^{13}C_{org\text{-}DICeq}$ averaging −20‰ (Figure S6). This may have several explanations: (i) Lower DIC concentrations and $CO_{2(aq)}$ availability in Alberca result in transport-limited rather than carboxylation-limited fixation, and thus a smaller isotope fractionation (e.g., Pardue et al. 1976; Close and Henderson 2020). This was also suggested for similarly less depleted isotopic signatures of Alberca planktonic organic matter relative to the other Mexican lakes (Havas et al. 2023a). (ii) Possibly slower CO_2 diffusion through the microbial mat of Alberca microbialites, which would result in a smaller apparent C isotope fractionation recorded by the biomass (e.g., Des Marais et al. 1989; Louyakis et al. 2017). (iii) A higher proportion of green sulfur bacteria (GSB) in the biomass of Alberca microbialites relative to the other lakes (Iniesto, Moreira, Reboul, et al. 2021). The GSB use the reverse tricarboxylic acid (TCA) cycle which tends to induce smaller C isotope fractionations than organisms using the Calvin-Benson-Bassham (CCB) pathway (Hayes 2001). We also reported the imprint of GSB on Lake Alberca planktonic and dissolved organic matter isotope signals (Havas et al. 2023a, 2023b).

Bulk organic C isotope signatures are in agreement with metabarcoding data which suggest that the microbial community in the microbialites of the four lakes are dominated by oxygenic and anoxygenic photosynthesis (Saghaï et al. 2015; Valdespino-Castillo et al. 2018; Iniesto, Moreira, Reboul, et al. 2021). By contrast, other metabolisms favoring carbonate precipitation such as microbial sulfate-reduction were shown to represent a minor fraction of the microbial communities (Saghaï et al. 2015, 2016; Iniesto, Moreira, Benzerara, et al. 2021, Iniesto, Moreira, Reboul, et al. 2021).

5.2 | Assessing if Microbialite Carbonates Precipitate in Isotopic Equilibrium With Their Environment

The microbialites from different lakes predominantly group in distinctive clusters in a $\delta^{13}C$–$\delta^{18}O$ plot (Figure 6), supporting the hypothesis that they record the specific conditions of the different locations and/or different pathways of formation. Their respective mineralogy partly explains the observed isotopic signatures. For example, the much higher $\delta^{13}C$–$\delta^{18}O$ values recorded in the white microbialites (Figure 6) are consistent with hydromagnesite precipitation (dominant in that facies), as it induces C and O isotope fractionations larger by ~2.1‰ and 2.8‰ than those recorded by aragonite, respectively (Table S3; Aharon 1988; Romanek et al. 1992; Kim et al. 2007; Harrison et al. 2021). The isotopic variability recorded in the microbialite carbonates also reflects the differences in the lakes water isotopic signals $\delta^{13}C_{DIC}$ and $\delta^{18}O_{H_2O}$, controlled by distinct basement rock compositions, groundwater flow paths, evaporation rates, and potential volcanic degassing (see 2.2; Havas et al. 2023a).

However, most $\delta^{13}C_{DIC\text{-}eq}$ and some $\delta^{18}O_{H_2O\text{-}eq}$ deviate from the measured lake water compositions (Figure 6b), showing that not all the microbialites are in isotopic equilibrium with the current lake waters even after considering their respective carbonates mineralogy (Figure 9). Note that the effect of temperature (within the range relevant to these lakes) is negligible on the carbonate C isotope signatures but is predominant on O isotopes. Considering temperatures of carbonate precipitation lower than the estimated yearly average water temperatures by 2°C–4°C, the $\Delta^{18}O_{H_2O\text{-}eq}$ recorded by microbialites are closer to 0‰ (i.e., closer to equilibrium) (Figure S2). Nonetheless, some of the microbialites would require to have precipitated at unlikely low surface average temperatures of 14°C to be in equilibrium with their lake water (Figure S2). Indeed, Macek et al. (2020) report temperatures that have almost always been above 14.5°C at depths above 20 m in Alchichica from 2003 to 2016. Our temperature data from May 2019 and October 2022 in Alchichica do not fall below 15°C at any depth. Instead, surface water temperatures are almost consistently above 17°C (Macek et al. 2020; this study). The available data for the other lakes show similar temperature depth profiles (or even warmer in Alberca).

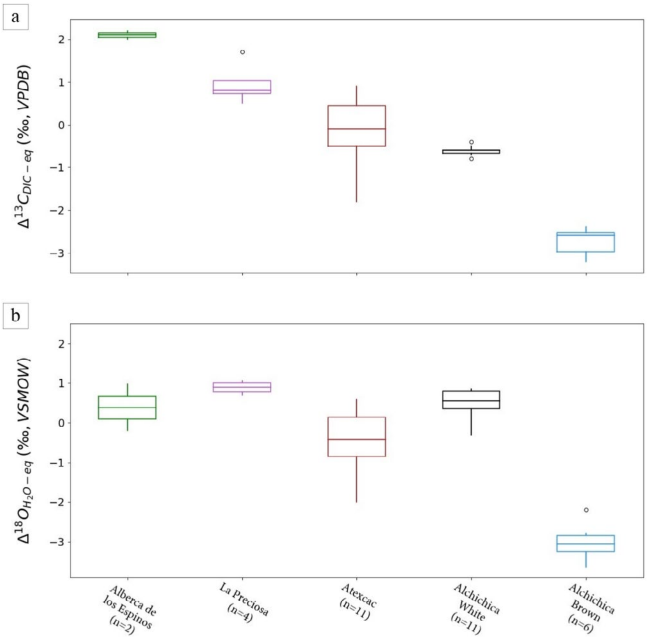

FIGURE 9 | Boxplots of the $\Delta^{13}C_{DIC\text{-}eq}$ and $\Delta^{18}O_{H_2O\text{-}eq}$ parameters for the main microbialite groups. These parameters represent the respective offset between the isotopic compositions of DIC (a) and H_2O (b) in equilibrium with the bulk microbialite carbonates and DIC and H_2O actually measured in each lake. The boxes extend from the lower to upper quartile values; the line in the middle corresponds to the median; the whiskers extend from min to max values excluding potential outlier data. For surface microbialites, we use an average temperature of 18°C for the SOB lakes, and 20°C for Lake Alberca.

Another possible explanation for $\Delta^{13}C_{DIC\text{-}eq}$ and $\Delta^{18}O_{H_2O\text{-}eq}$ departing from null values is that the studied microbialites precipitated from a lake water with different isotopic signatures than those sampled. For example, this could be the case if microbialites formed in waters that had experienced more evaporation or dilution than the present waters. Indeed, the bulk of microbialite carbonates represents a time-integrated history, by contrast with the punctual measurements of water chemistry. Therefore, microbialites may have formed from an evolving lake water. In that case $\Delta^{13}C_{DIC\text{-}eq}$ and $\Delta^{18}O_{H_2O\text{-}eq}$ may be expected to covary within a single environment. However, we see that the $\Delta^{13}C_{DIC\text{-}eq}$ offsets do not correlate with $\Delta^{18}O_{H_2O\text{-}eq}$ (Figure 9). In more detail, we find that $\Delta^{13}C_{DIC\text{-}eq}$ and $\Delta^{18}O_{H_2O\text{-}eq}$ strongly correlate only for Atexcac microbialites ($R^2 = 0.91$; Figure 10), which indeed suggest hydrologic changes in that lake (Section 5.5), while the 'Alberca', 'La Preciosa', and 'Alchichica white' microbialite groups do not show such a $\Delta^{13}C_{DIC\text{-}eq}$–$\Delta^{18}O_{H_2O\text{-}eq}$ covariation (Figure 10). A slight covariation for the 'Alchichica brown' samples can be explained by the effect of external water sources on these microbialites (Section 5.3.3). Finally, the measured water and DIC isotope compositions could vary with depth and sampling season. For carbon, however, considering the lakes $\delta^{13}C_{DIC}$ measured at any depth (Section 4.5) would not change the direction of $\Delta^{13}C_{DIC\text{-}eq}$ deviations. For instance, in Alberca and La Preciosa, it would increase even further the $\Delta^{13}C_{DIC\text{-}eq}$ recorded by their microbialites. Also, carbonates in the surficial

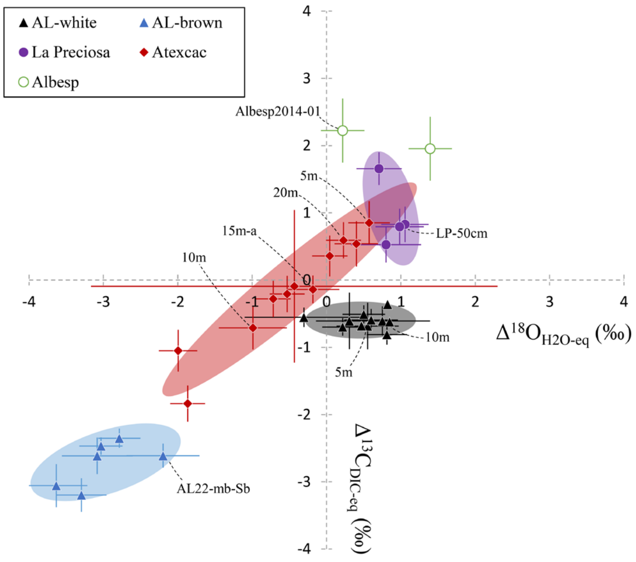

FIGURE 10 | Cross-plot of $\Delta^{13}C_{DIC\text{-}eq}$ as a function of $\Delta^{18}H_2O_{\text{-}eq}$ for the five main microbialite groups. Active microbialites sampled underwater are labeled for each group. R^2 values for the 'AL-white', 'AL-brown', 'Atexcac', and 'La Preciosa' microbialite groups are 0.19 ($n = 11$), 0.38 ($n = 6$), 0.91 ($n = 11$), and 0.29 ($n = 4$), respectively (not calculated for Albesp as $n = 2$). Ellipses represent 95% confidence ellipses.

sediments at the bottom of the lakes record near isotopic equilibrium with the lakes $\delta^{13}C_{DIC}$ (Havas et al. 2023a), showing that the measured $\delta^{13}C_{DIC}$ are representative of yearly average values with little effects from seasonal variations. For oxygen, further evaluation of the inter-seasonal and depth variability of $\delta^{18}O_{H_2O}$ is required to assess whether it can explain the $\Delta^{18}O_{H_2O\text{-eq}}$ values. Overall, while the microbialite carbonate O isotope signals primarily record the lake water isotope signatures, the microbialites C isotope signals—recording different deviation from equilibrium values—reflect the variety of processes microbialites form through (see further details in sections 5.3.1, 5.3.2).

It can be noted that authigenic carbonates in microbialites may well be in isotopic equilibrium with their porewaters, but not with the overlying water (e.g., Leapaldt et al. 2024). Microbialite carbonates would thus mainly reflect the porewater and hence the internal microbialite system rather than its growth environment. The chemistry of porewaters in microbialites may be challenging to determine (especially in the fossil record), but comparing the microbialite carbonate records to the chemistry of water columns then allows assessing the main drivers of the microbialite machinery. Hence, by combining the geological, microbiological, and geochemical data, we discuss further how the microbialite carbonate isotopic data inform us about the microbialites environment and the internal processes influencing their formation.

5.3 | Carbon Isotopes in Microbialite Carbonates

5.3.1 | An Autotrophic Signature Recorded in the Microbialite Carbonates From Relatively Low Alkalinity Lakes: Alberca and La Preciosa

Microbialites from Alberca and La Preciosa lakes show strictly positive $\Delta^{13}C_{DIC\text{-eq}}$ offsets (Figure 9). This ^{13}C-enrichment of the microbialite carbonates relative to equilibrium with the surrounding DIC can be interpreted as the effect of autotrophic activity on carbonate precipitation (e.g., Nitti et al. 2012; Louyakis et al. 2017; White III et al. 2020). For example, photosynthesis increases pH via the consumption of ^{12}C-rich CO_2, which results in ^{12}C-poor HCO_3^- ions in the surrounding solution and favors carbonate precipitation recording positive $\Delta^{13}C_{DIC\text{-eq}}$. In La Preciosa, the connection between microbial activity and the positive C isotope shift of carbonates is also directly evidenced by micro-drilling in one of the samples ('PR-2'). In this microbialite, while the $\delta^{13}C$–$\delta^{18}O$ signatures of "detrital carbonates" infilling the porosity and lake bottom sediments overlap, the microbialite shrubs show systematic ^{13}C-enrichments but similar $\delta^{18}O$ values to the other two groups (Figure 7). The $\delta^{13}C_{DIC\text{-eq}}$ and $\delta^{18}O_{H_2O\text{-eq}}$ of the porosity-filling 'H6' subsample, are lower than those measured in sediment samples, suggesting that this reworked material may have had a complex history departing from the modern lake water features (e.g., different hydrology regime, differential secondary alteration). By contrast, the signatures of 'H8' and 'H7' lean toward the microbial shrubs composition, suggesting that porosity-filling grains represent a mixture between "abiotic" pelagic carbonates and reworked microbial carbonates (Figure 7). This highlights as previously suggested that analyzing multiple carbonate facies within a single sample may prove powerful to further discriminate the processes of microbialite formation (e.g., McCormack and Kwiecien 2021; Leapaldt et al. 2024).

Interestingly, the positive $\Delta^{13}C_{DIC\text{-eq}}$ biosignatures are preserved in the carbonates of Alberca and La Preciosa microbialites—mainly Mg-calcite and aragonite, respectively—which are not necessarily primary phases. Indeed, monohydrocalcite and/or poorly crystalline Mg-silicates were shown to precipitate as metastable precursor phases before secondary Mg-calcite and/or aragonite in these lakes (Zeyen et al. 2015, 2021). Microfossils of autotrophic organisms (cyanobacteria, green algae, diatoms) were observed mainly associated with the precursor phases and may have influenced their precipitation (Zeyen et al. 2015, 2021). Yet, in La Preciosa microbialites, part of the aragonite was also suggested to form primarily without a precursor phase (Zeyen et al. 2015). Two interesting non-exclusive conclusions can be drawn from this. First, if Mg-calcite and aragonite are primary, the fact that they record a positive $\Delta^{13}C_{DIC\text{-eq}}$ biosignature means that their precipitation may also be linked to autotrophic activity. Second, if they form as secondary replacement of a metastable precursor phase, this early diagenetic replacement still allows for the preservation of a primary ^{13}C-enrichment biosignature.

5.3.2 | Alchichica "White Microbialites": Physico-Chemically and Possibly Heterotrophy-Driven Carbonate Precipitation

The $\Delta^{13}C_{DIC\text{-eq}}$ of the white facies microbialites in Alchichica averages -0.6 ± 0.1‰ (Figure 9a) suggesting that their bulk carbonates (mainly hydromagnesite) precipitate close to equilibrium, with a slight depletion in (heavy) ^{13}C relative to the lake DIC. In these microbialites, hydromagnesite was either suggested to precipitate due to supersaturation of the lake water and (i-a) random and abiotic replacement of aragonite and/or (i-b) nucleation on the microbial cells or (ii), heterotrophic degradation of the EPS and release of Mg^{2+} cations (Kaźmierczak et al. 2011; Gérard et al. 2013).

The $\Delta^{13}C_{DIC\text{-eq}}$ values close to 0‰ in Alchichica support that hydromagnesite could precipitate mainly from physico-chemical supersaturation, overprinting the isotopic signal of primary aragonite that precipitates in the vicinity of the microbial mat at the microbialites surfaces (Figure 4g, i; Figure 5b,c). Among the lakes studied, only the waters of Alchichica are consistently supersaturated with respect to amorphous Mg-carbonate (Zeyen et al. 2021; Figure S7) which may be a prerequisite for hydromagnesite precipitation. Indeed, hydromagnesite unlikely precipitates primarily but rather after the formation of more hydrated and soluble precursor phases such as nesquehonite and dypingite (Chaka 2018; Zeyen et al. 2021). As a result, hydromagnesite is found as the major constituent of the massive microbialite deposits in Alchichica (Figure 2) while only being reported as a small fraction of a single microbialite sample in Atexcac (Zeyen et al. 2021). Note that all these hydrated Mg-carbonate phases have very similar chemical composition and should induce similar C isotope fractionations (Aharon 1988; Harrison et al. 2021). A small difference in the isotopic fractionation between magnesite and dypingite/hydromagnesite (≤ 0.2‰; see Section 3.5) may explain some of the white microbialites $\Delta^{13}C_{DIC\text{-eq}}$ variability, but it does not cover the entire range of values reported for this facies.

Yet, the slightly negative $\Delta^{13}C_{DIC\text{-}eq}$ values suggest the incorporation into the white microbialite of carbonates derived from the degradation of organic C. Depletion of heavy ^{13}C in microbialite carbonates relative to equilibrium with the surrounding DIC is commonly interpreted as the effect of heterotrophic activity on carbonate precipitation. Notably, anaerobic respiration processes such as MSR generate ^{12}C-rich HCO_3^- ions via the oxidation of organic matter, which would result in negative $\Delta^{13}C_{DIC\text{-}eq}$ carbonates (e.g., Andres et al. 2006; Breitbart et al. 2009; Nitti et al. 2012). Though the microbial diversity in a microbialite is not necessarily representative of the organisms that drove their formation (Petryshyn et al. 2021), we note that the proportion of microbial heterotrophs that favor carbonatogenesis (including sulfate reducers) is minor in Alchichica microbialites (Saghaï et al. 2015; Iniesto, Moreira, Benzerara, et al. 2021, Iniesto, Moreira, Reboul, et al. 2021). In contrast, these microbialites contain a significant abundance of aerobic heterotrophs and fermenters that may contribute to the degradation of organic-C and its incorporation into hydromagnesite. Organic-C remineralization may also be achieved by photosynthetic organisms that carry fermentation at night (Visscher and Stolz 2005). Some of these photosynthetic organisms could correspond to the green endolithic cyanobacterial layer found within several white microbialites of Alchichica (e.g., ‘AL-T-7’ in Figure 2). Although the metabolic activities mentioned above should all favor carbonate dissolution via an acidification of the medium instead of precipitation (e.g., Dupraz et al. 2009), the high alkalinity of the lake may buffer such variations and still allow hydromagnesite precipitation. Moreover, these heterotrophic processes may facilitate hydromagnesite precipitation by releasing Mg^{2+} ions bound to EPS during the degradation of the mats (Dupraz et al. 2004, 2009).

Couradeau et al. (2013) and Gérard et al. (2013) demonstrated that aragonite at the surface of Alchichica white microbialites was specifically precipitated by cyanobacteria from the Pleurocapsales order. This is not seen in the bulk carbonate isotopic signal of white microbialites as they contain minor amounts of aragonite compared with hydromagnesite. Organic-C respiration and related acidification could lead to aragonite dissolution, and as noted above, to hydromagnesite precipitation. A similar process has been evidenced in Pavilion Lake microbialites, where the initial ^{13}C-enriched biosignatures of surficial carbonates resulting from photosynthesis activity are erased by secondary precipitation toward the microbialite's core (Belan et al. 2019). The secondary carbonates were suggested to precipitate in equilibrium with the lake bulk DIC, and/or under the local influence of heterotrophy-derived DIC. A replacement of aragonite by hydromagnesite would also explain the scarcity (or loss) of biogenic remains within the pervasive hydromagnesite matrixes (Figure 4g–i), and the low TOC content of the white facies, which is about half that of the brown facies. However, whereas the slight $\Delta^{13}C_{DIC\text{-}eq}$ depletion in Alchichica white microbialite carbonates evidences that their net C budget includes C coming from organic matter remineralization, it cannot fully discriminate between the different metabolisms performing this remineralization (e.g., aerobic respiration vs. fermentation) and the different pathways of carbonate precipitation (physico-chemical oversaturation vs. cation release from EPS degradation).

Overall, hydromagnesite precipitation in Alchichica is mostly bolstered by the lake's physico-chemical conditions with a proportionally small possible contribution from heterotrophy-driven DIC, as suggested by their carbonate content close to 100%, and the C isotope signatures close to equilibrium with lake $\delta^{13}C_{DIC}$ and consistently with the very poor preservation of biogenic remains in the hydromagnesite core of white microbialites. The isotopic signature of biotically induced aragonite precipitates is overridden by this more massive and non-metabolically driven hydromagnesite precipitation. Respiratory processes may further favor the formation of hydromagnesite despite the fact the microbial communities in Alchichica microbialites contain a predominant abundance of photoautotrophic organisms.

5.3.3 | Microbialites as Local Environmental Recorders: Alchichica “Brown” Facies Records Local Fluid Sources

A first explanation for the marked negative $\Delta^{13}C_{DIC\text{-}eq}$ measured for aragonitic brown microbialites in Alchichica could be that aragonite precipitation is fed by inorganic carbon resulting from respiratory processes. Here we favor a second explanation: the negative bulk $\Delta^{13}C_{DIC\text{-}eq}$ in Alchichica brown microbialites is due to the local seepage of underground fluids. Several arguments support this hypothesis: (i) rapid bubbling rising from discrete spots on the columnar brown microbialites has been observed (Saghaï et al. 2015), which could result from groundwater reaching the lake on the western and southern shore (Figure 8; Silva Aguilera 2019), and/or from the release of volcanic-fluids. (ii) Brown microbialites form specifically on the western side of the lake, often harboring a columnar morphology, whereas the white microbialites—mostly containing hydromagnesite—form all around the lake (Figure S8). (iii) The Eu anomaly (Eu*), TOC, and trace metal element contents all show higher values in the brown microbialites than in white microbialites (Tables S4 and S5; Figure 5b,c vs. 5d). The high Fe content of brown microbialites has been in particular interpreted as the result of the local seepage of anoxic Fe-rich groundwater that leached Fe out from the volcanic rocks in the crater's wall and basement (Zeyen et al. 2019). In this regard, the location of brown microbialites specifically on the western shore of Alchichica is most likely favored by the proximity of outcropping volcanic rocks from the crater wall (Figure S8). Last, (iv), the geochemical analyses performed on groundwater inflowing the lake support the hypothesis of an external source impacting the formation of brown microbialites. Several lines of argument validate that groundwater and infiltrating runoff water directly impacts the brown microbialites' mineralogy, element and isotopic geochemistry. First, although the inflowing groundwater is overall less saturated with respect to carbonates than the lake water (Table S2), it is especially undersaturated with hydromagnesite ($SI_{HMG} = -5.7$ at Pz-20) but saturated with aragonite ($SI_{ara} = 1$ at Pz-20) as it approaches and enters Alchichica (Figure 8). Groundwater would thus favor aragonite precipitation over hydromagnesite. Second, the Mg/Ca ratio evolves from less than 2 in the groundwater to ~100 in the lake water (Table S2), which has a critical influence on the mineralogy of carbonates (e.g., Müller et al. 1972; Chagas et al. 2016). Comparing more than 10 Mexican lakes including those studied here, Zeyen et al. (2021) found that hydromagnesite was present in their microbialites for Mg/Ca ratios above ~50, and aragonite for Mg/Ca ratios above ~3. Therefore, these external groundwater sources would favor a dominant precipitation of aragonite over hydromagnesite (the latter being observed elsewhere in the lake). Finally, the $\delta^{13}C_{DIC}$ and $\delta^{18}O_{H_2O}$ of groundwater have more negative values than the lake water, and thus nicely explain both the negative $\Delta^{13}C_{DIC\text{-}eq}$ and $\Delta^{18}O_{H_2O\text{-}eq}$ offsets recorded by the brown facies (Figure 9). We note that these data do not allow distinguishing the influence of groundwater/infiltrating runoff-water versus volcanic escape fluids, which would also carry a negative $\delta^{13}C_{DIC}$, Fe-rich and Eu-rich signatures.

5.3.4 | Synthesis and Conceptual Model for the Overall Controls on Microbialite C Isotope Signatures

The Mexican microbialite carbonates record very diverse isotopic signatures (Figure 6). These are partly explained by interlake variability in water and DIC isotope compositions (Beeler et al. 2020; Havas et al. 2023a), but important isotopic variations appear even within a single environment. For example, the brown microbialites in Alchichica record the inputs of external (and localized) fluid sources from runoff, groundwater, and possibly volcanic fluids. Additionally, distinct carbonate mineralogical assemblages—including calcite, aragonite, and hydromagnesite—induce several permil differences in the microbialite isotopic compositions. Even when all these parameters are considered, the C isotope signatures range from slightly depleted to markedly enriched in ^{13}C relative to equilibrium-predicted values (Figure 9a). These offsets reflect the set of environmental constraints that impact the microbialites isotopic record, sometimes dominated by biotic or abiotic factors (Figure 11).

The positive $\Delta^{13}C_{DIC\text{-}eq}$ consistent with autotrophic carbonate precipitation are only found in Alberca and La Preciosa microbialites, although the microbial communities are dominated by photoautotrophic organisms in the microbialites of all four lakes (Iniesto, Moreira, Reboul, et al. 2021). We note however, that the trend of $\Delta^{13}C_{DIC\text{-}eq}$ values recorded by the microbialites of the four lakes (Figure 9a) follows the alkalinity gradient linking the four lake waters (Zeyen et al. 2021; Havas et al. 2023a). This suggests a primary role of the environmental parameters that control this inter-lake alkalinity gradient on the microbialites C isotope record as detailed below.

In Alchichica—the lake with the highest alkalinity—massive precipitation of hydromagnesite favors the record of $\Delta^{13}C_{DIC\text{-}eq}$ close to equilibrium and carbonate contents close to 100%. The slightly negative values of $\Delta^{13}C_{DIC\text{-}eq}$ (Figure 11) show that some of the carbonates originate from the remineralization of organic-C, which suggests that respiratory processes may foster the precipitation of hydromagnesite (Section 5.3.2). By contrast, the least alkaline lakes Alberca and La Preciosa record positive $\Delta^{13}C_{DIC\text{-}eq}$ shifts consistent with an autotrophy-dominated carbonatogenesis (Iniesto, Moreira, Reboul, et al. 2021), and correlating with lower carbonate/TOC ratios (Figure 11a,b). In between, Atexcac samples complete the trend, showing that the more carbonates precipitate, the closer they get to isotopic values in equilibrium with their surrounding waters (Figure 11a). In Alberca, La Preciosa, and Atexcac microbialites, organic remains are primarily associated with Mg-silicates (Zeyen et al. 2015, 2021) and the microbialites with higher Mg-silicate contents record more positive shifts in their carbonate C isotopic signals, imparted to the activity of autotrophs (Figure 11). By contrast, subsequent replacement carbonates precipitate due to physico-chemical oversaturation (from non-metabolically mediated DIC) and/or the oxidation of the organic matter, bringing $\Delta^{13}C_{DIC\text{-}eq}$ closer to 0‰ (similarly to the process described for Alchichica white microbialites). Consistently, more positive $\Delta^{13}C_{DIC\text{-}eq}$ are recorded as the microbialites TOC content increases, and decreasing $\Delta^{13}C_{DIC\text{-}eq}$ are recorded toward low TOC and Mg-silicate contents, and high carbonate content (Figure 11). Thus, despite similar microbial community structures (Iniesto, Moreira, Reboul, et al. 2021), microbialite carbonates may

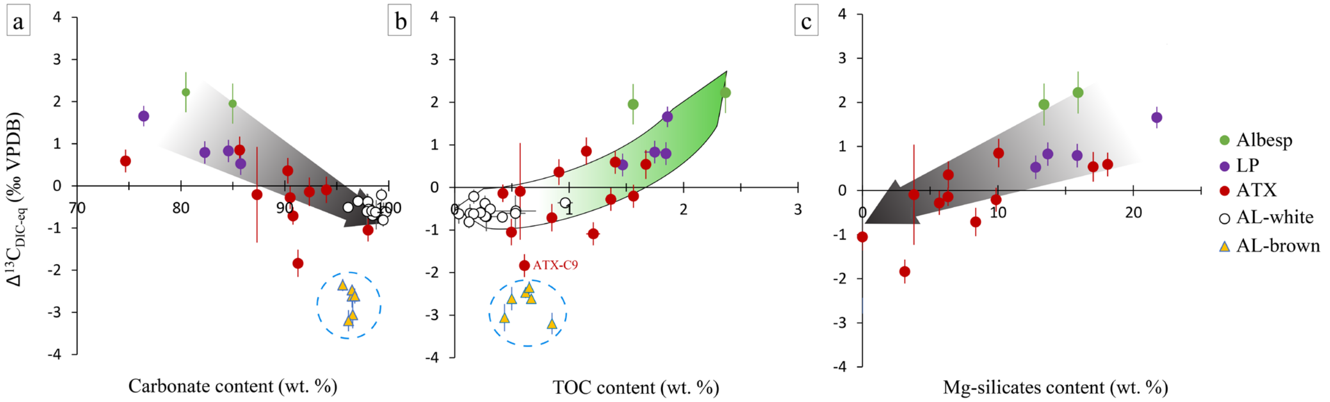

FIGURE 11 | Isotopic disequilibrium between the lakes $\delta^{13}C_{DIC}$ and microbialites $\delta^{13}C_{DIC\text{-}eq}$ as a function of the microbialites bulk carbonate (a), total organic carbon (b), and Mg-silicate (c) contents, all in weight percent (wt. %). Microbialites carbonates with $\Delta^{13}C_{DIC\text{-}eq}$ close to 0 precipitate near equilibrium with the lakes $\delta^{13}C_{DIC}$; those deviating from 0 have been affected by other processes (autotrophic influence on carbonatogenesis in La Preciosa) or sources (e.g., "brown" aragonitic microbialites in Alchichica). These deviations have more or less chance to be expressed and preserved depending on the alkalinity-buffer capacity of each lake water, and how much carbonates precipitate at equilibrium. The carbonate and Mg-silicate contents are anti-correlated, supports that the latter may be replaced by the precipitation of carbonates, which is accompanied by a loss of primary $\Delta^{13}C_{DIC\text{-}eq}$ offsets. The gray-shaded areas represent the trends of Mg-silicate replacement (in c) by carbonate precipitation (in a). Alchichica microbialites are not represented in 'c' as Mg-silicates were not identified in these samples. Sample 'ATX-C9' plots relatively off the trends, but may be affected by secondary alteration as it was collected at the limit where many weathered microbialites occurred.

or may not record isotopic biosignatures, depending on the buffering capacity of the DIC reservoir due to high alkalinity levels and more or less important physico-chemical carbonate precipitation. Similar inferences were drawn about the DIC isotope variations in the water column of the Mexican lakes (Havas et al. 2023a). Note that by "physico-chemical precipitation", we refer to carbonates that form from a DIC pool that was not isotopically affected by C fixation, but accumulated due to abiotic factors (e.g., evaporation, volcanic degassing); it does not preclude a biological influence, for example via the action of EPS favoring heterogeneous nucleation and precipitation. These results suggest that microbialites forming in highly alkaline water bodies are weakly susceptible to preserve diagnostic C isotopic biosignatures in their carbonates, providing a limit condition for using them as adequate isotopic proxies of microbial activity.

Importantly, it shows that even positive or negative deviations from isotopic equilibrium do not inform on the microbial community specific composition. Indeed, the microbial diversity of the Mexican microbialites (and microbialites in general) is composed of a multitude of organisms and metabolisms which can promote carbonate precipitation at different times (e.g., day and night cycles) and locations (e.g., niches within biofilms). Instead, the $\Delta^{13}C_{DIC\text{-}eq}$ offsets reflect the difference between the amount of organic C stored in the microbialite from autotrophic fixation and that remineralized by heterotrophic activity, which can be defined as the microbialites net primary productivity (mNPP). On top of that, the isotopic shift generated by the mNPP budget may be preserved or suppressed according to the alkalinity content and the susceptibility of the lake water to promote carbonate formation due to physico-chemical precipitation (PCp) (Figure 12). The PCp can be defined as the amount of C in carbonates precipitated from non-biologically-cycled DIC, which is allowed when solutions are highly super-saturated. If carbonate precipitation occurs in a highly alkaline, DIC-buffered water and is dominated by PCp, the carbonates will be close to isotopic equilibrium with the water (trend B in Figure 12). These "equilibrium" carbonates can also represent detrital grain infilling the microbialite. If net primary (i.e., autotrophic) production is significantly positive, it will generate a ^{13}C-rich ambient DIC and favor carbonate precipitation (trend A in Figure 12). If heterotrophic remineralization of organic-C initially fixed by autotrophy is quantitative (mNPP back to 0), it will result in a net null isotopic mass balance following trend 1 in Figure 12 (with mNPP/PCp tending to 0 due to mNPP). Trend 1 can also occur if PCp takes over precipitation from biologically-cycled DIC, leading to isotopic compositions at equilibrium. If a decrease of mNPP due to organic matter respiration leads to carbonate precipitation from the respiration-associated DIC and a partial dissolution and loss of the primary carbonates ('A' or 'B' in Figure 12), it will lead to slightly negative $\Delta^{13}C_{dic\text{-}eq}$ (trends 2 or 2′, respectively). A substantial dissolution of the primary carbonates will favor more negative $\Delta^{13}C_{dic\text{-}eq}$ signatures (following trends 3 and 3′). Note that trends 3 and 3′ reflect a low contribution of "equilibrium carbonate", which would otherwise bring the $\Delta^{13}C_{dic\text{-}eq}$ closer back to 0‰ (trends 2/2′). Overall, in high alkalinity-DIC environments, the carbonate $\Delta^{13}C_{dic\text{-}eq}$ signatures should be buffered toward 0‰, while in lower alkalinity-DIC setting, they will be modulated by the mNPP; low or high mNPP values suggesting heterotrophy- or autotrophy-dominated carbonate precipitation at the bulk scale, respectively.

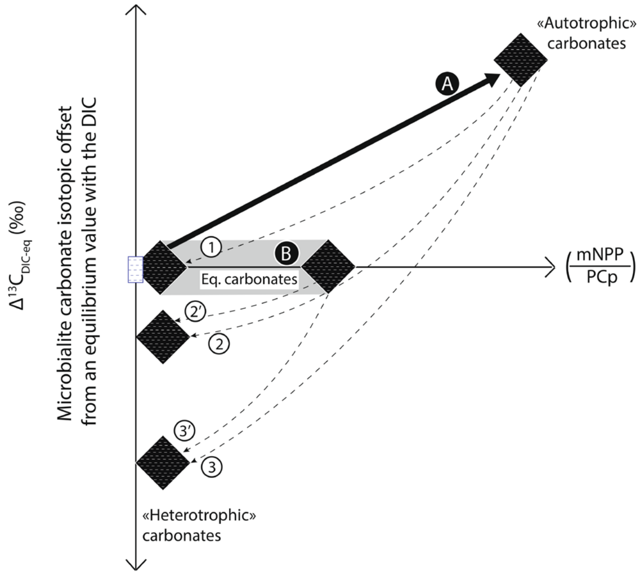

FIGURE 12 | Conceptual model for the relation between the C isotope offset to equilibrium values recorded by microbialite carbonates ($\Delta^{13}C_{DIC\text{-}eq}$ in ‰) and the ratio of the microbialite net primary productivity to physico-chemical carbonate precipitation (mNPP/PCp). Positive and negative $\Delta^{13}C_{DIC\text{-}eq}$ imply that the microbialite carbonate precipitated from ^{13}C-enriched and ^{13}C-depleted DIC relative to ambient $\delta^{13}C_{DIC}$, respectively. The mNPP can be defined as the difference between the amount of organic C stored in the microbialite from autotrophic fixation and that which is remineralized by heterotrophic activity. Yet, this mNPP budget does not provide insights into the specific composition of the microbial community, the locus (e.g., associated to autotrophs or heterotrophs) or time (e.g., day or night) of precipitation. The PCp can be defined as the amount of C in carbonates precipitated from non-biologically-cycled DIC, which is allowed when solutions are highly super-saturated. Overall, this suggests that the microbialites bulk carbonate C isotope composition provides a time-integrated estimate of the ratio between mNPP and PCp. In high alkalinity-DIC environments, the carbonate C isotope signatures should be buffered toward 0‰ due to important PCp, while in lower alkalinity-DIC setting, they will be modulated by the mNPP (see Section 5.3.4 for more details).

5.4 | Oxygen Isotopes in Microbialite Carbonates

Microbialites from Alberca, La Preciosa, and the white facies in Alchichica show slightly positive $\Delta^{18}O_{H_2O\text{-}eq}$; Atexcac samples are characterized by a wide range of values around 0‰, whereas Alchichica brown microbialites show strictly negative offsets (Figure 9b; Table S5). Microbial carbonate O isotope compositions are generally found to precipitate in equilibrium with their surrounding waters and thus mostly reflect hydrologic and climatic phenomena (Arenas et al. 2019; Ingalls et al. 2020). The $\Delta^{18}O_{H_2O\text{-}eq}$ recorded here support this conclusion, but allow discussing the parameters that may superimpose onto these phenomena.

5.4.1 | Potential Biases in the Determination of $\delta^{18}O_{H_2O\text{-}eq}$ and $\Delta^{18}O_{H_2O\text{-}eq}$

A single study previously determined the O-isotope fractionation associated with the precipitation of hydromagnesite, and no specific acid fractionation factor (during its isotopic analysis) was determined for this phase (O'Neil and Barnes 1971; Kim et al. 2015). Therefore, considering the complexity of the chemical formula of hydromagnesite with respect to oxygen ($Mg_5(CO_3)_4(OH)_2 \cdot 4H_2O$), it is possible that (i) isotopic exchange with H_3PO_4 acid during samples pre-analysis treatment leads to inaccurate $\delta^{18}O$ measurements, and/or (ii) the intrinsic fractionation associated with hydromagnesite precipitation is influenced by a number of parameters that were not tested by O'Neil and Barnes (1971) pioneering work. For example, the effect of salinity on hydromagnesite O isotope compositions remains to be determined. Indeed, the effect of salinity on calcite O isotopes was demonstrated by Kim and O'Neil (1997), who found that the O isotope fractionation related to calcite precipitation ($\alpha_{\text{calcite-HO}}$) increases with solutes concentration (Ca^{2+} and DIC), at a given temperature. At 20°C and a DIC concentration of 25 mM, they showed that this fractionation was about 2‰ heavier in the case of equilibrium (Zeebe 1999). They estimated that equilibrium fractionation occurs at DIC concentrations close to that of Lake Alberca (5 mM). Interestingly, the immersed calcitic microbialite sample of Lake Alberca has a $\delta^{18}O_{carb}$ in equilibrium with the lake $\delta^{18}O_{H_2O}$ (Table S5).

No salt effect on aragonite O isotope compositions was found for solutions with ionic strengths up to 700 mmol/kg (Kim et al. 2007, 2014). Thus, the slight ^{18}O-enrichment in La Preciosa microbialites cannot be explained by a salt effect.

On top of mineralogy and salinity, changes in the fluid composition with space and time may also bias the interpretation of $\delta^{18}O_{H_2O\text{-eq}}$ and $\Delta^{18}O_{H_2O\text{-eq}}$. In Alchichica, the ^{18}O-depleted signatures of the brown microbialites reinforce the interpretation based on C isotope that their precipitation occurs where external underground water sources seep into the lake (Section 5.3.3). The $\delta^{18}O_{H_2O\text{-eq}}$ values calculated for this facies are not as negative as those of the groundwaters (−11.7‰ for Pz-20), suggesting that brown microbialites precipitate from the mixing between underground sources and the lake water, which is also suggested by the slight covariation observed between $\Delta^{13}C_{\text{DIC-eq}}$ and $\Delta^{18}O_{H_2O\text{-eq}}$ (Figure 10).

In Atexcac, the clear correlation between $\Delta^{13}C_{\text{DIC-eq}}$ and $\Delta^{18}O_{H_2O\text{-eq}}$, and the negative and positive $\Delta^{18}O_{H_2O\text{-eq}}$ offsets are well explained by the fact that these microbialites precipitated from a lake water at varying evaporation degrees (Section 5.5). The fact that only one of the four Atexcac samples in the water is in equilibrium with the current lake $\delta^{18}O_{H_2O}$ (Table S5) suggests that these microbialites precipitated at distinct times in the past, during more or less evaporated conditions. Additionally, the speleothem-like fabric found in a sample collected at a 20-m depth (Figure S3) suggests that some of the submerged samples may originate from a higher vertical position and recently fell along the crater wall before being collected (Figure 2).

5.4.2 | Putative Biological Effect on Carbonate O Isotopes

The different DIC species bear very distinct O isotope signatures, with $\delta^{18}O_{HCO3}$ higher than $\delta^{18}O_{CO3}$ and $\delta^{18}O_{H_2O}$ by about 16‰ and 34‰ at equilibrium, respectively (Zeebe 1999). Offsets between microbialites $\delta^{18}O_{carb}$ and equilibrium-predicted $\delta^{18}O$ values have thus been related by several authors to pH variations under the influence of biological activity (Andres et al. 2006; Louyakis et al. 2017). Metabolisms inducing higher pH and carbonate precipitation should lead to a larger incorporation of CO_3^{2-} into the carbonate minerals, and thus decrease the $\delta^{18}O_{carb}$ values (Zeebe 1999). However, the microbialites studied here record a $\delta^{18}O_{carb}$ higher than expected from the lakes $\delta^{18}O_{H_2O}$. A kinetic isotope effect related to fast precipitation rates would lead $\delta^{18}O_{carb}$ to lower instead of higher values (Kim et al. 2006). Nevertheless, we suggest that under a local biologically-mediated increase of pH, conversion of HCO_3^- to CO_3^{2-} and preferential incorporation of CO_3^{2-} into the solid carbonate matrix (Kim et al. 2006) could participate in the high $\delta^{18}O_{carb}$ values observed. Because O isotope equilibration time between water, carbonate, and bicarbonate ions is relatively long (e.g., 10 and 100 h at pHs of 8.3 and 10.3, respectively, vs. ~30 s for C isotopes at pH 8.3; Zeebe and Wolf-Gladrow 2001), newly formed ^{18}O-rich CO_3^{2-} ions would incorporate the carbonate minerals before they have reequilibrated with the water $\delta^{18}O_{H_2O}$—thereby generating both ^{13}C- and ^{18}O-enriched signatures in the precipitate.

Previous studies showed that biogenic aragonite tends to induce slightly larger departures from water isotope compositions than abiogenic aragonite, even though their O isotope fractionation-temperature relationships are statistically indistinguishable (Kim et al. 2007 and references therein). The slight offset from equilibrium fractionations recorded by biogenic aragonite has been described as a species-specific "vital effect" (Kim et al. 2007). In Alchichica white microbialites, the specific association between aragonite precipitates and cyanobacterial lineages (Couradeau et al. 2013; Gérard et al. 2013) suggests that a "vital effect" could potentially deviate the microbialites $\delta^{18}O$ from equilibrium-expected values. In Alberca and La Preciosa, we evidenced the influence of microbial activity on the microbialite carbonate isotope signatures of C (Section 5.3.1). We also showed the link between the biologically-influenced precipitation of Mg-silicates and replacement by authigenic carbonates (Section 5.3.4), which could potentially affect the microbialite carbonate isotope signatures of O. Thus, an impact of biology on the microbialite carbonate O isotope compositions cannot be fully excluded, although other abiotic factors are more prevalent in these signatures.

5.5 | Climatic and Hydrological Records by Microbialite Carbonates

Continental microbialite isotopic records have commonly been used as paleoclimate archives, to constrain parameters such as paleo-temperatures and hydrology (Frantz et al. 2014; Newell et al. 2017; Arenas et al. 2019; Ingalls et al. 2020). The microbialites studied here form in an evaporitic closed basin and were sampled within intervals spanning several meters in height (Table 2). In Alberca and La Preciosa, they would thus be expected to show $\delta^{13}C$–$\delta^{18}O$ correlations typical of evaporation trends (Talbot 1990), while in Atexcac and Alchichica such correlation may be hindered by high alkalinity levels (Li and Ku 1997). The microbialite record is however contrasted regarding this evaporation isotopic trend, highlighting the processes that can blur the climatic record of microbialite carbonates.

In La Preciosa, no correlation is found (Figure 6), and most of the isotopic variability is recorded in $\delta^{13}C_{carb}$, suggesting a dominant biological influence (Section 5.3.1). Although the number of samples is limited, the highest $\delta^{13}C$ value is measured in the most emerged sample ('PR-3', at ~3 m above the current water level), opposite to what is expected from a less evaporated context, and likely related to biological influence on carbonate formation instead.

Atexcac microbialites record a clear correlation between $\delta^{13}C_{carb}$ and $\delta^{18}O_{carb}$ ($R^2 = 0.88$; Figure 6a). Both $\delta^{13}C_{carb}$ and $\delta^{18}O_{carb}$ increase going downward from the most emerged sample, about 6 m above current water level, to a microbialite collected 5 m below current water level within the lake (Table S5). This trend strongly suggests that microbialites record the progressive evaporation of the lake, which led to a substantial volume decrease in Atexcac (Figure 2). Although they may record different time periods, we notice that the slope recorded by Atexcac microbialites (slope $m = 0.87$; Figure 6a,b) is much higher than that recorded by the bottom lake sediments of the same lake ($m = 0.30$; Table S6), as well as the sediments of La Preciosa (m = 0.42; Figure 7, Table S6). Therefore, while the $\delta^{13}C_{DIC\text{-}eq}$–$\delta^{18}O_{H_2O\text{-}eq}$ covariation in Atexcac microbialites mostly reflects hydrological changes in the lake, its slope may also vary with biological influence. Consistently, biological activity has more chances to affect the $\delta^{13}C$–$\delta^{18}O$ covariation recorded by microbialites carbonates than that recorded by pelagic sediments, especially for $\delta^{13}C$ (cf. Figure 7 and Section 5.3.1).

The carbonate isotopic record of Alchichica microbialites was previously interpreted to reflect different stages of formation at distinct evaporation levels (Kaźmierczak et al. 2011). However, we showed above that the correlation seen in our $\delta^{13}C_{carb}$–$\delta^{18}O_{carb}$ dataset actually reflects the existence of two microbialite endmembers having separate pathways of formation, and mineralogy (Figure S8). Paleoclimatic studies showed that emerged brown microbialites (estimated at ~1100 years BP by Kaźmierczak et al. 2011) actually formed at a period of severe droughts in the SOB area (e.g., Bhattacharya et al. 2015). The evaporation interpretation is also at odds with the contiguous arrangement of "brown" and "white" samples (Figure S8), or the fact that presently forming brown microbialites bear the same isotopic signal ('AL22-mb-Sb') as emerged ones.

In Alchichica white microbialites, whereas a weak correlation is found between the $\delta^{13}C_{carb}$ and $\delta^{18}O_{carb}$ signatures, it disappears when considering the isotopic compositions of their fluid of precipitation (i.e., $\delta^{13}C_{DIC\text{-}eq}$ and $\delta^{18}O_{H_2O\text{-}eq}$; Figure 6, R^2 of 0.44 vs. 0.003). It illustrates the importance of accounting for the mineralogy of carbonates. In Eocene stromatolites from the Green River Formation, different carbonate facies were interpreted to record drastic evaporation and hydrological changes based on ^{13}C- and ^{18}O-isotope- and Na-enrichments found in micrite layers (Frantz et al. 2014). However, all samples from these micrite layers are composed of dolomite, or calci-dolomite, while the other facies contains only calcite. This change of mineralogy (instead of evaporation) could explain at least part of the isotopic variations measured. At 20°C, dolomite and calcite would precipitate with a ~5‰-difference in $\delta^{18}O$ (Chacko et al. 2001 and references therein). Similarly, dolomite was found to incorporate much higher proportions of Na than calcite at room temperature (Oomori et al. 1985). It underlines that small isotopic variations in the geological record, for instance in Precambrian formations containing different carbonates mineralogy (e.g., Tang et al. 2022), should be interpreted with caution.

Despite major evaporation occurring in the area of Alchichica (Silva-Aguilera et al. 2022), the white microbialites isotopic record shows little variability, with standard deviations of ±0.1 and 0.3‰ for $\delta^{13}C_{DIC\text{-}eq}$ and $\delta^{18}O_{H_2O\text{-}eq}$, respectively. For C, it may relate to the high alkalinity and DIC concentrations of the lake which buffers its DIC isotope composition (Li and Ku 1997; Havas et al. 2023a). For O, it suggests that the temperature and hydrological conditions in which they form were similar to those prevailing today. Accordingly, paleoclimate indicators from the SOB area suggest that about 3000 years ago (when emerged white microbialites would have formed, Kaźmierczak et al. 2011) the climate may have been similar as today (Bhattacharya et al. 2015). It is also possible that hydromagnesite continually reequilibrates with the lake water, especially for O isotopes, which would not allow the preservation of lake changing O isotope compositions.

Importantly, all microbialites from the SOB area record markedly more positive isotopic signatures than if they were in equilibrium with the aquifer waters. For example, a fully aragonitic microbialite would record $\delta^{13}C_{carb}$ and $\delta^{18}O_{carb}$ around −0.3‰ and −10.8‰, respectively, if it precipitated from the aquifer water (at 18°C, considering the average composition of the three wells reported in this study). The microbialite carbonates are thus all sensitive to the evaporitic nature of their basin when considering the composition of the water sources (e.g., water from the aquifer), but not necessarily when focusing on the microbialites from a single lake (as they may record only a specific time interval of the basin's history). This was previously suggested for other types of lacustrine sedimentary carbonate records as well (Horton et al. 2016). It reminds that raw $\delta^{13}C$ and $\delta^{18}O$ of microbialite carbonates are primarily related to the isotopic compositions of the sources they precipitate from. It also shows the importance of zooming out from the microbial deposits and analyzing the isotopic signatures at the scale of a basin in order to retrieve a climatic message from microbialite formations.

Overall, we conclude that a clear record of a basin's hydrologic conditions in microbialite carbonates is favored by, or requires: a large volume of water evaporation, a continuous distribution of microbialites along vertical/time transects, DIC concentrations low enough to prevent buffering effects (i.e., not as in Alchichica), and mineralogical compositions immune to isotopic exchange and reequilibration (i.e., not as with hydromagnesite). Microbialites should be analyzed in parallel to proxies for the composition of the basins water sources bearing in mind that $\delta^{13}C$–$\delta^{18}O$ relationships may be impacted by biological activity.

6 | Conclusion

Our study brings to light the diversity of processes that may affect the isotopic record of microbialite carbonates, comparing four modern volcanic lakes where microbialites forming through different pathways are found. Using an extended dataset on the microbialites' mineralogy, petrography, and geochemistry, we discriminated biotic and abiotic factors influencing their formation. In essence, the microbialite carbonate C and O isotope signatures primarily record the composition of the fluid they precipitate from, but C isotopes also record the microbialite net primary productivity budget (mNPP) in conjunction with physico-chemical precipitation (PCp) related to the water alkalinity levels.

Primary isotopic biosignatures are mainly found as ^{13}C-enrichments in the carbonates of the lakes with the lowest alkalinity contents, suggesting a direct influence of autotrophic microorganisms during carbonate precipitation. By contrast, carbonate precipitation under high DIC and cation concentrations shows isotopic signals close to equilibrium with the lake water and/or slightly ^{13}C-depleted. This suggests major non-metabolically driven precipitation processes and a possible enhancer role by respiration activities, which in turn depend on primary production, indicating the entanglement of biogeological processes and intricacy of the isotopic record. These results support that the role of biology in high DIC environments is dominated by the process of capturing/releasing divalent cations on/away from EPS, or creating nucleation points, rather than changing the pH and alkalinity levels, as suggested before (Arp et al. 2001).

Although the initial replacement of precursor phases (either metastable silicates or carbonates) by more stable and crystalline carbonate phases permits the preservation of C isotope biosignatures, we find that further transformation of the precursors correlates with a loss of primary biosignatures. Therefore, the preservation or loss of isotopic (and potentially morphological) biosignatures in microbialite carbonates is highly contingent on the environmental context of their formation, independently of the microbial community.

Microbialite oxygen isotope compositions are primarily related to the basin hydrological regime and the processes/sources affecting its water isotopic signatures. Biotic effects on O isotopes of microbialite carbonates are not excluded but seem minor. Further knowledge on O isotope behavior upon the formation of poorly documented carbonate phases such as hydromagnesite will help refining our understanding of microbialite O isotope signals.

Overall, this work highlights the importance of integrating petrographic, mineralogical, and geological context information for the interpretation of ancient microbialite geochemical data. Besides, it shows that finding a good proxy of the average isotopic composition in the fluid surrounding the microbialites is crucial to properly understand the isotopic signatures of authigenic carbonates and provide pertinent paleoenvironment constraints. Surrounding sediments, and “detrital grains” within microbialites porosity are good targets to provide such a complementary record.

Acknowledgements

This research was supported by the Agence Nationale de la Recherche (France, grant no. ANR-18-CE02-0013-02). The authors thank Ivan Jovovic, Ludovic Bruneau, Anne-Lise Santoni, and the GISMO platform (Biogéosciences, Université de Bourgogne, UMR CNRS 6282, France). We thank Christophe Durlet for the µXRF analyses on the Morphoptics platform in Dijon. We thank Céline Liorzou and Bleuenn Guéguen for the analyses at the Pôle Spectrométrie Océan (Laboratoire Géo-Océan, Brest, France) and Laure Cordier for the ion chromatography analyses at IPGP (France). JC was funded by a grant from the Interface pour le vivant doctorate programme at Sorbonne Université.

Conflicts of Interest

The authors declare no conflicts of interest.

Data Availability Statement

The data that supports the findings of this study are available in the Supporting Information of this article.

References

Aharon, P. 1988. “A Stable-Isotope Study of Magnesites From the Rum Jungle Uranium Field, Australia: Implications for the Origin of Strata-Bound Massive Magnesites.” *Chemical Geology* 69: 127–145. https://doi.org/10.1016/0009-2541(88)90164-7.

Alcocer, J., M. Merino-Ibarra, J. A. Ramírez-Zierold, et al. 2022. “Physicochemical Characteristics.” In *In Lake Alchichica Limnology: The Uniqueness of a Tropical Maar Lake*, 101–142. Springer International Publishing. https://doi.org/10.1007/978-3-030-79096-7_7.

Andres, M. S., D. Y. Sumner, R. P. Reid, and P. K. Swart. 2006. “Isotopic Fingerprints of Microbial Respiration in Aragonite From Bahamian Stromatolites.” *Geology* 34: 973. https://doi.org/10.1130/G22859A.1.

Antunes, G. C., L. V. Warren, J. Okubo, et al. 2022. “The Rise and Fall of the Giant Stromatolites of the Lower Permian Irati Formation (Paraná Basin, Brazil): A Multi-Proxy Based Paleoenvironmental Reconstruction.” *Palaeogeography, Palaeoclimatology, Palaeoecology* 606: 111246. https://doi.org/10.1016/j.palaeo.2022.111246.

Arenas, C., M. C. Osácar, L. Auqué, and C. Sancho. 2019. “Coupling Textural and Stable-Isotope Variations in Fluvial Stromatolites: Comparison of Pleistocene and Recent Records in NE Spain.” *Journal of Palaeogeography* 8: 13. https://doi.org/10.1186/s42501-019-0021-y.

Armienta, M. A., G. Vilaclara, S. De la Cruz-Reyna, et al. 2008. “Water Chemistry of Lakes Related to Active and Inactive Mexican Volcanoes.” *Journal of Volcanology and Geothermal Research* 178: 249–258. https://doi.org/10.1016/j.jvolgeores.2008.06.019.

Arp, G., A. Reimer, and J. Reitner. 2001. “Photosynthesis-Induced Biofilm Calcification and Calcium Concentrations in Phanerozoic Oceans.” *Science* 292: 1701–1704. https://doi.org/10.1126/science.1057204.

Assayag, N., K. Rivé, M. Ader, D. Jézéquel, and P. Agrinier. 2006. “Improved Method for Isotopic and Quantitative Analysis of Dissolved Inorganic Carbon in Natural Water Samples.” *Rapid Communications in Mass Spectrometry* 20: 2243–2251. https://doi.org/10.1002/rcm.2585.

Bahniuk, A. M., S. Anjos, A. B. França, et al. 2015. “Development of Microbial Carbonates in the Lower Cretaceous Codó Formation (North-East Brazil): Implications for Interpretation of Microbialite Facies Associations and Palaeoenvironmental Conditions.” *Sedimentology* 62: 155–181. https://doi.org/10.1111/sed.12144.

Beeler, S. R., F. J. Gomez, and A. S. Bradley. 2020. “Controls of Extreme Isotopic Enrichment in Modern Microbialites and Associated Abiogenic Carbonates.” *Geochimica et Cosmochimica Acta* 269: 136–149. https://doi.org/10.1016/j.gca.2019.10.022.

Belan, M. A., A. L. Brady, S.-T. Kim, D. S. S. Lim, and G. F. Slater. 2019. “Spatial Distribution and Preservation of Carbon Isotope Biosignatures in Freshwater Microbialite Carbonate." *ACS Earth and Space Chemistry* 3: 335–343. https://doi.org/10.1021/acsearthspacechem.8b00182.

Bhattacharya, T., R. Byrne, H. Böhnel, et al. 2015. "Cultural Implications of Late Holocene Climate Change in the Cuenca Oriental, Mexico." *Proceedings of the National Academy of Sciences* 112, no. 6: 1693–1698. https://doi.org/10.1073/pnas.1405653112.

Bougeault, C., C. Durlet, E. Vennin, et al. 2020. "Variability of Carbonate Isotope Signatures in a Hydrothermally Influenced System: Insights From the Pastos Grandes Caldera (Bolivia)." *Minerals* 10, no. 11: 989. https://doi.org/10.3390/min10110989.

Brady, A. L., G. F. Slater, C. R. Omelon, et al. 2010. "Photosynthetic Isotope Biosignatures in Laminated Micro-Stromatolitic and Non-laminated Nodules Associated With Modern, Freshwater Microbialites in Pavilion Lake, B.C." *Chemical Geology* 274: 56–67. https://doi.org/10.1016/j.chemgeo.2010.03.016.

Breitbart, M., A. Hoare, A. Nitti, et al. 2009. "Metagenomic and Stable Isotopic Analyses of Modern Freshwater Microbialites in Cuatro Ciénegas, Mexico." *Environmental Microbiology* 11: 16–34. https://doi.org/10.1111/j.1462-2920.2008.01725.x.

Buongiorno, J., F. J. Gomez, D. A. Fike, and L. C. Kah. 2018. "Mineralized Microbialites as Archives of Environmental Evolution, Laguna Negra, Catamarca Province, Argentina." *Geobiology* 17, no. 2: gbi.12327. https://doi.org/10.1111/gbi.12327.

Burne, R. V., and L. S. Moore. 1987. "Microbialites: Organosedimentary Deposits of Benthic Microbial Communities." *PALAIOS* 2: 241–254. https://doi.org/10.2307/3514674.

Carrasco-Núñez, G., J. Hernández, J. Cavazos-Álvarez, et al. 2021. "Volcanic Geology of the Easternmost Sector of the Trans-Mexican Volcanic Belt, Mexico." *Journal of Maps* 17: 486–496. https://doi.org/10.1080/17445647.2021.1970037.

Carrasco-Núñez, G., M. H. Ort, and C. Romero. 2007. "Evolution and Hydrological Conditions of a Maar Volcano (Atexcac Crater, Eastern Mexico)." *Journal of Volcanology and Geothermal Research* 159: 179–197. https://doi.org/10.1016/j.jvolgeores.2006.07.001.

Chacko, T., D. R. Cole, and J. Horita. 2001. "Equilibrium Oxygen, Hydrogen and Carbon Isotope Fractionation Factors Applicable to Geologic Systems." In *Stable Isotope Geochemistry*, edited by J. W. Valley and D. R. Cole, 1–82. De Gruyter. https://doi.org/10.1515/9781501508745-004.

Chagas, A. A. P., G. E. Webb, R. V. Burne, and G. Southam. 2016. "Modern Lacustrine Microbialites: Towards a Synthesis of Aqueous and Carbonate Geochemistry and Mineralogy." *Earth-Science Reviews* 162: 338–363. https://doi.org/10.1016/j.earscirev.2016.09.012.

Chaka, A. M. 2018. "Ab Initio Thermodynamics of Hydrated Calcium Carbonates and Calcium Analogues of Magnesium Carbonates: Implications for Carbonate Crystallization Pathways." *ACS Earth and Space Chemistry* 2: 210–224. https://doi.org/10.1021/acsearthspacechem.7b00101.

Chako Tchamabé, B., G. Carrasco-Núñez, D. P. Miggins, and K. Németh. 2020. "Late Pleistocene to Holocene Activity of Alchichica Maar Volcano, Eastern Trans-Mexican Volcanic Belt." *Journal of South American Earth Sciences* 97: 102404. https://doi.org/10.1016/j.jsames.2019.102404.

Chakrabarti, G., D. Shome, S. Kumar, J. S. Armstrong-Altrin, and A. N. Sial. 2011. "Carbon and Oxygen Isotopic Variations in Stromatolitic Dolomites of Palaeoproterozoic Vempalle Formation, Cuddapah Basin, India." *Carbonates and Evaporites* 26: 181–191. https://doi.org/10.1007/s13146-011-0054-5.

Chédeville, C., M.-N. Guilbaud, and C. Siebe. 2020. "Stratigraphy and Radiocarbon Ages of Late-Holocene Las Derrumbadas Rhyolitic Domes and Surrounding Vents in the Serdán-Oriental Basin (Mexico): Implications for Archeology, Biology, and Hazard Assessment." *Holocene* 30: 402–419. https://doi.org/10.1177/0959683619887417.

Close, H. G., and L. C. Henderson. 2020. "Open-Ocean Minima in δ13C Values of Particulate Organic Carbon in the Lower Euphotic Zone." *Frontiers in Marine Science* 7: 540165. https://doi.org/10.3389/fmars.2020.540165.

Corkeron, M., G. E. Webb, J. Moulds, and K. Grey. 2012. "Discriminating Stromatolite Formation Modes Using Rare Earth Element Geochemistry: Trapping and Binding Versus In Situ Precipitation of Stromatolites From the Neoproterozoic Bitter Springs Formation, Northern Territory, Australia." *Precambrian Research* 212: 194–206. https://doi.org/10.1016/j.precamres.2012.04.019.

Couradeau, E., K. Benzerara, E. Gérard, et al. 2013. "Cyanobacterial Calcification in Modern Microbialites at the Submicrometer Scale." *Biogeosciences* 10: 5255–5266. https://doi.org/10.5194/bg-10-5255-2013.

Della Porta, G. 2015. "Carbonate Build-Ups in Lacustrine, Hydrothermal and Fluvial Settings: Comparing Depositional Geometry, Fabric Types and Geochemical Signature." *Geological Society, London, Special Publications* 418, no. 1: 17–68. https://doi.org/10.1144/SP418.4.

Des Marais, D. J., H. Nguyen, M. Cheatham, T. Cheatham, E. Munoz, and Y. Cohen. 1989. "Carbon Isotopic Trends in the Hypersaline Ponds and Microbial Mats at Guerrero Negro, Baja California Sur, Mexico-Implications for Precambrian Stromatolites." In *Microbial Mats: Physiological Ecology of Benthic Microbial Communities*, edited by Y. Cohen and E. Rosenberg, 191–203. American Society for Microbiology.

Döbelin, N., and R. Kleeberg. 2015. "Profex: A Graphical User Interface for the Rietveld Refinement Program BGMN." *Journal of Applied Crystallography* 48, no. 5: 1573–1580. https://doi.org/10.1107/S1600576715014685.

Dupraz, C., R. P. Reid, O. Braissant, A. W. Decho, R. S. Norman, and P. T. Visscher. 2009. "Processes of Carbonate Precipitation in Modern Microbial Mats." *Earth-Science Reviews* 96: 141–162. https://doi.org/10.1016/j.earscirev.2008.10.005.

Dupraz, C., P. T. Visscher, L. K. Baumgartner, and R. P. Reid. 2004. "Microbe–Mineral Interactions: Early Carbonate Precipitation in a Hypersaline Lake (Eleuthera Island, Bahamas)." *Sedimentology* 51: 745–765. https://doi.org/10.1111/j.1365-3091.2004.00649.x.

Ferrari, L., T. Orozco-Esquivel, V. Manea, and M. Manea. 2012. "The Dynamic History of the Trans-Mexican Volcanic Belt and the Mexico Subduction Zone." *Tectonophysics* 522: 122–149. https://doi.org/10.1016/j.tecto.2011.09.018.

Fischer, W. W., S. Schroeder, J. P. Lacassie, et al. 2009. "Isotopic Constraints on the Late Archean Carbon Cycle From the Transvaal Supergroup Along the Western Margin of the Kaapvaal Craton, South Africa." *Precambrian Research* 169: 15–27. https://doi.org/10.1016/j.precamres.2008.10.010.

Frantz, C. M., V. A. Petryshyn, P. J. Marenco, A. Tripati, W. M. Berelson, and F. A. Corsetti. 2014. "Dramatic Local Environmental Change During the Early Eocene Climatic Optimum Detected Using High Resolution Chemical Analyses of Green River Formation Stromatolites." *Palaeogeography, Palaeoclimatology, Palaeoecology* 405: 1–15. https://doi.org/10.1016/j.palaeo.2014.04.001.

Friesenbichler, E., S. Richoz, A. Baud, et al. 2018. "Sponge-Microbial Build-Ups From the Lowermost Triassic Chanakhchi Section in Southern Armenia: Microfacies and Stable Carbon Isotopes." *Palaeogeography, Palaeoclimatology, Palaeoecology* 490: 653–672. https://doi.org/10.1016/j.palaeo.2017.11.056.

Gérard, E., B. Ménez, E. Couradeau, et al. 2013. "Specific Carbonate–Microbe Interactions in the Modern Microbialites of Lake Alchichica (Mexico)." *ISME Journal* 7: 1997–2009. https://doi.org/10.1038/ismej.2013.81.

Grey, K., and S. M. Awramik. 2020. *Handbook for the Study and Description of MICROBIALITES*, Geological Survey of Western Australia, 147. Geological Survey of Western Australia: Bulletin.

Grotzinger, J. P. 1990. “Geochemical model for Proterozoic Stromatolite Decline.” *American Journal of Science* 290-A: 80–103.

Harrison, A. L., P. Bénézeth, J. Schott, E. H. Oelkers, and V. Mavromatis. 2021. “Magnesium and Carbon Isotope Fractionation During Hydrated mg-Carbonate Mineral Phase Transformations.” *Geochimica et Cosmochimica Acta* 293: 507–524. https://doi.org/10.1016/j.gca.2020.10.028.

Havas, R., C. Thomazo, M. Iniesto, et al. 2023b. “The Hidden Role of Dissolved Organic Carbon in the Biogeochemical Cycle of Carbon in Modern Redox-Stratified Lakes.” *Biogeosciences* 20: 2405–2424. https://doi.org/10.5194/bg-20-2405-2023.

Havas, R., C. Thomazo, M. Iniesto, et al. 2023a. “Biogeochemical Processes Captured by Carbon Isotopes in Redox-Stratified Water Columns: A Comparative Study of Four Modern Stratified Lakes Along an Alkalinity Gradient.” *Biogeosciences* 20: 2347–2367. https://doi.org/10.5194/bg-20-2347-2023.

Hayes, J. M. 2001. “Fractionation of Carbon and Hydrogen Isotopes in Biosynthetic Processes.” *Reviews in Mineralogy and Geochemistry* 43: 225–278. https://doi.org/10.1515/9781501508745-006.

Hohl, S. V., and S. Viehmann. 2021. “Stromatolites as Geochemical Archives to Reconstruct Microbial Habitats Through Deep Time: Potential and Pitfalls of Novel Radiogenic and Stable Isotope Systems.” *Earth-Science Reviews* 218: 103683. https://doi.org/10.1016/j.earscirev.2021.103683.

Horton, T. W., W. F. Defliese, A. K. Tripati, and C. Oze. 2016. “Evaporation Induced 18O and 13C Enrichment in Lake Systems: A Global Perspective on Hydrologic Balance Effects.” *Quaternary Science Reviews* 131: 365–379. https://doi.org/10.1016/j.quascirev.2015.06.030.

Houghton, J., D. Fike, G. Druschel, V. Orphan, T. M. Hoehler, and D. J. Des Marais. 2014. “Spatial Variability in Photosynthetic and Heterotrophic Activity Drives Localized δ 13 C Org Fluctuations and Carbonate Precipitation in Hypersaline Microbial Mats.” *Geobiology* 12: 557–574. https://doi.org/10.1111/gbi.12113.

Hren, M. T., and N. D. Sheldon. 2020. “Terrestrial Microbialites Provide Constraints on the Mesoproterozoic Atmosphere.” *Depositional Record* 6: 4–20. https://doi.org/10.1002/dep2.79.

Ingalls, M., C. M. Frantz, K. E. Snell, and E. J. Trower. 2020. “Carbonate Facies-Specific Stable Isotope Data Record Climate, Hydrology, and Microbial Communities in Great Salt Lake, UT.” *Geobiology* 18: 566–593. https://doi.org/10.1111/gbi.12386.

Ingalls, M., H. C. Leapaldt, and M. K. Lloyd. 2024. “Microbial Autotrophy Recorded by Carbonate Dual Clumped Isotope Disequilibrium.” *Geochemistry, Geophysics, Geosystems* 25, no. 6: e2024GC011590. https://doi.org/10.1029/2024GC011590.

Iniesto, M., D. Moreira, K. Benzerara, et al. 2021. “Rapid Formation of Mature Microbialites in Lake Alchichica, Mexico.” *Environmental Microbiology Reports* 13: 600–605. https://doi.org/10.1111/1758-2229.12957.

Iniesto, M., D. Moreira, G. Reboul, et al. 2021. “Core Microbial Communities of Lacustrine Microbialites Sampled Along an Alkalinity Gradient.” *Environmental Microbiology* 23: 51–68. https://doi.org/10.1111/1462-2920.15252.

Kaźmierczak, J., S. Kempe, B. Kremer, P. López-García, D. Moreira, and R. Tavera. 2011. “Hydrochemistry and Microbialites of the Alkaline Crater Lake Alchichica, Mexico.” *Facies* 57: 543–570. https://doi.org/10.1007/s10347-010-0255-8.

Khelen, A. C., C. Manikyamba, S. Ganguly, et al. 2017. “Geochemical and Stable Isotope Signatures of Proterozoic Stromatolitic Carbonates From the Vempalle and Tadpatri Formations, Cuddapah Supergroup, India: Implications on Paleoenvironment and Depositional Conditions.” *Precambrian Research* 298: 365–384. https://doi.org/10.1016/j.precamres.2017.05.021.

Kim, S.-T., T. B. Coplen, and J. Horita. 2015. “Normalization of Stable Isotope Data for Carbonate Minerals: Implementation of IUPAC Guidelines.” *Geochimica et Cosmochimica Acta* 158: 276–289. https://doi.org/10.1016/j.gca.2015.02.011.

Kim, S.-T., C. K. Gebbinck, A. Mucci, and T. B. Coplen. 2014. “Oxygen Isotope Systematics in the Aragonite–CO_2–H_2O–NaCl System up to 0.7mol/Kg Ionic Strength at 25°C.” *Geochimica et Cosmochimica Acta* 137: 147–158. https://doi.org/10.1016/j.gca.2014.02.050.

Kim, S.-T., C. Hillaire-Marcel, and A. Mucci. 2006. “Mechanisms of Equilibrium and Kinetic Oxygen Isotope Effects in Synthetic Aragonite at 25°C.” *Geochimica et Cosmochimica Acta* 70: 5790–5801. https://doi.org/10.1016/j.gca.2006.08.003.

Kim, S.-T., and J. R. O'Neil. 1997. “Equilibrium and Nonequilibrium Oxygen Isotope Effects in Synthetic Carbonates.” *Geochimica et Cosmochimica Acta* 61: 3461–3475. https://doi.org/10.1016/S0016-7037(97)00169-5.

Kim, S.-T., J. R. O'Neil, C. Hillaire-Marcel, and A. Mucci. 2007. “Oxygen Isotope Fractionation Between Synthetic Aragonite and Water: Influence of Temperature and Mg_2+ Concentration.” *Geochimica et Cosmochimica Acta* 71: 4704–4715. https://doi.org/10.1016/j.gca.2007.04.019.

Kshirsagar, P., C. Siebe, M. N. Guilbaud, and S. Salinas. 2016. “Geological and Environmental Controls on the Change of Eruptive Style (Phreatomagmatic to Strombolian-Effusive) of Late Pleistocene El Caracol Tuff Cone and Its Comparison With Adjacent Volcanoes Around the Zacapu Basin (Michoacán, México).” *Journal of Volcanology and Geothermal Research* 318: 114–133. https://doi.org/10.1016/j.jvolgeores.2016.03.015.

Kshirsagar, P., C. Siebe, M. N. Guilbaud, S. Salinas, and P. W. Layer. 2015. “Late Pleistocene Alberca de Guadalupe Maar Volcano (Zacapu Basin, Michoacán): Stratigraphy, Tectonic Setting, and Paleo-Hydrogeological Environment.” *Journal of Volcanology and Geothermal Research* 304: 214–236. https://doi.org/10.1016/j.jvolgeores.2015.09.003.

Leapaldt, H. C., C. M. Frantz, J. Olsen-Valdez, K. E. Snell, E. J. Trower, and M. Ingalls. 2024. “Primary to Post-Depositional Microbial Controls on the Stable and Clumped Isotope Record of Shoreline Sediments at Fayetteville Green Lake.” *Geobiology* 22: e12609. https://doi.org/10.1111/gbi.12609.

Lelli, M., T. G. Kretzschmar, J. Cabassi, et al. 2021. “Fluid Geochemistry of the Los Humeros Geothermal Field (LHGF – Puebla, Mexico): New Constraints for the Conceptual Model.” *Geothermics* 90: 101983. https://doi.org/10.1016/j.geothermics.2020.101983.

Lepot, K. 2020. “Signatures of Early Microbial Life From the Archean (4 to 2.5 Ga) eon.” *Earth-Science Reviews* 209: 103296. https://doi.org/10.1016/j.earscirev.2020.103296.

Li, H.-C., and T.-L. Ku. 1997. “δ13C–δ18C Covariance as a Paleohydrological Indicator for Closed-Basin Lakes.” *Palaeogeography, Palaeoclimatology, Palaeoecology* 133: 69–80. https://doi.org/10.1016/S0031-0182(96)00153-8.

Lorenz, V. 1986. “On the Growth of Maars and Diatremes and Its Relevance to the Formation of Tuff Rings.” *Bulletin of Volcanology* 48: 265–274. https://doi.org/10.1007/BF01081755.

Louyakis, A. S., J. M. Mobberley, B. E. Vitek, et al. 2017. “A Study of the Microbial Spatial Heterogeneity of Bahamian Thrombolites Using Molecular, Biochemical, and Stable Isotope Analyses.” *Astrobiology* 17: 413–430. https://doi.org/10.1089/ast.2016.1563.

Macek, M., X. S. Medina, A. Picazo, et al. 2020. “*Spirostomum Teres*: A Long Term Study of an Anoxic-Hypolimnion Population Feeding Upon Photosynthesizing Microorganisms.” *Acta Protozoologica* 59: 13–38. https://doi.org/10.4467/16890027AP.20.002.12158.

McCormack, J., and O. Kwiecien. 2021. “Coeval Primary and Diagenetic Carbonates in Lacustrine Sediments Challenge Palaeoclimate

Interpretations." *Scientific Reports* 11: 7935. https://doi.org/10.1038/s41598-021-86872-1.

Müller, G., G. Irion, and U. Förstner. 1972. "Formation and Diagenesis of Inorganic Ca- Mg Carbonates in the Lacustrine Environment." *Naturwissenschaften* 59: 158–164. https://doi.org/10.1007/BF00637354.

Newell, D. L., J. L. Jensen, C. M. Frantz, and M. D. Vanden Berg. 2017. "Great Salt Lake (Utah) Microbialite δ13C, δ18O, and δ15N Record Fluctuations in Lake Biogeochemistry Since the Late Pleistocene." *Geochemistry, Geophysics, Geosystems* 18: 3631–3645. https://doi.org/10.1002/2017GC007078.

Nitti, A., C. A. Daniels, J. Siefert, V. Souza, D. Hollander, and M. Breitbart. 2012. "Spatially Resolved Genomic, Stable Isotopic, and Lipid Analyses of a Modern Freshwater Microbialite From Cuatro Ciénegas, Mexico." *Astrobiology* 12: 685–698. https://doi.org/10.1089/ast.2011.0812.

O'Neil, J. R., and I. Barnes. 1971. "C13 and O18 Compositions in Some Fresh-Water Carbonates Associated With Ultramafic Rocks and Serpentinites: Western United States." *Geochimica et Cosmochimica Acta* 35: 687–697. https://doi.org/10.1016/0016-7037(71)90067-6.

Oomori, T., M. Nakasone, K. Kaneshima, and Y. Kitano. 1985. "Incorporation of Sodium Into Calcium Carbonate and Protodolomite." *Bulletin of the College of Science* 39: 51–56.

Pace, A., R. Bourillot, A. Bouton, et al. 2016. "Microbial and Diagenetic Steps Leading to the Mineralisation of Great Salt Lake Microbialites." *Scientific Reports* 6: 31495. https://doi.org/10.1038/srep31495.

Pardue, J. W., R. S. Scalan, C. Van Baalen, and P. L. Parker. 1976. "Maximum Carbon Isotope Fractionation in Photosynthesis by Blue-Green Algae and a Green Alga." *Geochimica et Cosmochimica Acta* 40, no. 3: 309–312. https://doi.org/10.1016/0016-7037(76)90208-8.

Pecoraino, G., W. D'Alessandro, and S. Inguaggiato. 2015. "The Other Side of the Coin: Geochemistry of Alkaline Lakes in Volcanic Areas." In *Volcanic Lakes, Advances in Volcanology*, edited by D. Rouwet, B. Christenson, F. Tassi, and J. Vandemeulebrouck, 219–237. Springer Berlin Heidelberg. https://doi.org/10.1007/978-3-642-36833-2_9.

Petryshyn, V. A., E. N. Junkins, B. W. Stamps, et al. 2021. "Builders, Tenants, and Squatters: The Origins of Genetic Material in Modern Stromatolites." *Geobiology* 19, no. 3: 261–277. https://doi.org/10.1111/gbi.12429.

Rendon-Lopez, M. J. 2008. "Limnologia fisica del lago crater los Espinos, Municipio de Jiménez Michoacan."

Riding, R. 2006. "Microbial Carbonate Abundance Compared With Fluctuations in Metazoan Diversity Over Geological Time." *Sedimentary Geology* 185: 229–238. https://doi.org/10.1016/j.sedgeo.2005.12.015.

Riding, R. 2011. "Microbialites, Stromatolites, and Thrombolites." In *Encyclopedia of Geobiology, Encyclopedia of Earth Sciences Series*, edited by J. Reitner and V. Thiel, 635–654. Springer Netherlands. https://doi.org/10.1007/978-1-4020-9212-1_196.

Romanek, C. S., E. L. Grossman, and J. W. Morse. 1992. "Carbon Isotopic Fractionation in Synthetic Aragonite and Calcite: Effects of Temperature and Precipitation Rate." *Geochimica et Cosmochimica Acta* 56: 419–430. https://doi.org/10.1016/0016-7037(92)90142-6.

Saghaï, A., Y. Zivanovic, D. Moreira, et al. 2016. "Comparative Metagenomics Unveils Functions and Genome Features of Microbialite-Associated Communities Along a Depth Gradient: Comparative Metagenomics of Microbialites From Lake Alchichica." *Environmental Microbiology* 18: 4990–5004. https://doi.org/10.1111/1462-2920.13456.

Saghaï, A., Y. Zivanovic, N. Zeyen, et al. 2015. "Metagenome-Based Diversity Analyses Suggest a Significant Contribution of Non-cyanobacterial Lineages to Carbonate Precipitation in Modern Microbialites." *Frontiers in Microbiology* 6: 797. https://doi.org/10.3389/fmicb.2015.00797.

Siebe, C., M.-N. Guilbaud, S. Salinas, and C. Chédeville-Monzo. 2012. "Eruption of Alberca de los Espinos tuff cone causes transgression of Zacapu lake ca. 25,000 yr BP in Michoacán, México." Presented at the IAS 4IMC Conference, Auckland, New Zeland, pp. 74–75.

Siebe, C., M.-N. Guilbaud, S. Salinas, et al. 2014. "Monogenetic volcanism of the Michoacán-Guanajuato Volcanic Field: Maar craters of the Zacapu basin and domes, shields, and scoria cones of the Tarascan highlands (Paracho-Paricutin region)." Presented at the Pre-meeting field guide for the 5th international Maar Conference, Querétaro, México, pp. 1–37.

Silva Aguilera, R. A. 2019. "Analisis del descenso del nivel de agua del lago Alchichica, Puebla, México 120."

Silva-Aguilera, R. A., G. Vilaclara, M. A. Armienta, and Ó. Escolero. 2022. *Hydrogeology and Hydrochemistry of the Serdán-Oriental Basin and the Lake Alchichica*, edited by J. Alcocer, 63–74. Springer International Publishing. Lake Alchichica Limnology. https://doi.org/10.1007/978-3-030-79096-7_5.

Talbot, M. R. 1990. "A Review of the Palaeohydrological Interpretation of Carbon and Oxygen Isotopic Ratios in Primary Lacustrine Carbonates." *Chemical Geology* 80: 261–279. https://doi.org/10.1016/0168-9622(90)90009-2.

Tang, P., D. Chen, Y. Wang, Y. Ding, M. El-Shafeiy, and B. Yang. 2022. "Diagenesis of Microbialite-Dominated Carbonates in the Upper Ediacaran Qigebrak Formation, NW Tarim Basin, China: Implications for Reservoir Development." *Marine and Petroleum Geology* 136: 105476. https://doi.org/10.1016/j.marpetgeo.2021.105476.

Valdespino-Castillo, P. M., R. J. Alcántara-Hernández, J. Alcocer, M. Merino-Ibarra, M. Macek, and L. I. Falcón. 2014. "Alkaline Phosphatases in Microbialites and Bacterioplankton From Alchichica Soda Lake, Mexico." *FEMS Microbiology Ecology* 2, no. 2014: 504–519. https://doi.org/10.1111/1574-6941.12411.

Valdespino-Castillo, P. M., P. Hu, M. Merino-Ibarra, et al. 2018. "Exploring Biogeochemistry and Microbial Diversity of Extant Microbialites in Mexico and Cuba." *Frontiers in Microbiology* 9: 510. https://doi.org/10.3389/fmicb.2018.00510.

Vennin, E., A. Bouton, R. Bourillot, et al. 2019. "The Lacustrine Microbial Carbonate Factory of the Successive Lake Bonneville and Great Salt Lake, Utah, USA." *Sedimentology* 66: 165–204. https://doi.org/10.1111/sed.12499.

Vennin, E., A. Bouton, A. Roche, et al. 2021. "The Limagne Basin: A Journey Through Modern and Fossil Microbial Deposits." *Bulletin de la Société Géologique de France* 192: 41. https://doi.org/10.1051/bsgf/2021030.

Vignale, F. A., D. Kurth, A. I. Lencina, et al. 2021. "Geobiology of Andean Microbial Ecosystems Discovered in Salar de Atacama, Chile." *Frontiers in Microbiology* 12: 762076. https://doi.org/10.3389/fmicb.2021.762076.

Visscher, P. T., and J. F. Stolz. 2005. "Microbial Mats as Bioreactors: Populations, Processes, and Products." In *Geobiology: Objectives, Concepts, Perspectives*, 87–100. Elsevier.

White, R. A., III, S. A. Soles, A. L. Brady, G. Southam, D. S. S. Lim, and G. F. Slater. 2020. "Biosignatures Associated With Freshwater Microbialites." *Life (Raleigh)* 10, no. 5: 66. https://doi.org/10.3390/life10050066.

Xu, B. 2011. "Microfacies, Carbon and Oxygen Isotopes of the Late Archean Stromatolitic Carbonate Platform of the Kaapvaal Craton, South Africa: Implications for Changes in Paleo-Environment." PhD diss., Ludwig-Maximilians-Universität München.

Zeebe, R. E. 1999. "An Explanation of the Effect of Seawater Carbonate Concentration on Foraminiferal Oxygen Isotopes." *Geochimica et Cosmochimica Acta* 63: 2001–2007. https://doi.org/10.1016/S0016-7037(99)00091-5.

Zeebe, R. E., and D. Wolf-Gladrow. 2001. *CO_2 in Seawater: Equilibrium, Kinetics, Isotopes*. Vol. 65. Gulf Professional Publishing.

Zeyen, N., K. Benzerara, O. Beyssac, et al. 2021. “Integrative Analysis of the Mineralogical and Chemical Composition of Modern Microbialites From Ten Mexican Lakes: What Do We Learn About Their Formation?” *Geochimica et Cosmochimica Acta* 305: 148–184. https://doi.org/10.1016/j.gca.2021.04.030.

Zeyen, N., K. Benzerara, J. Li, et al. 2015. “Formation of Low-T Hydrated Silicates in Modern Microbialites From Mexico and Implications for Microbial Fossilization.” *Frontiers in Earth Science* 3: 64. https://doi.org/10.3389/feart.2015.00064.

Zeyen, N., K. Benzerara, N. Menguy, et al. 2019. “Fe-Bearing Phases in Modern Lacustrine Microbialites From Mexico.” *Geochimica et Cosmochimica Acta* 253: 201–230. https://doi.org/10.1016/j.gca.2019.03.021.

Zhang, X.-Y., Y. Li, G. Wang, and H.-Q. Yang. 2021. “Different Accretion and Diagenetic Patterns Within the Fabrics of the Permian–Triassic Boundary Microbialites on the Leye Isolated Carbonate Platform, South China Block.” *Journal of Palaeogeography* 10, no. 1: 11. https://doi.org/10.1186/s42501-021-00091-3.

Zhu, D., Q. Liu, J. Wang, Q. Ding, and Z. He. 2021. “Stable Carbon and Oxygen Isotope Data of Late Ediacaran Stromatolites From a Hypersaline Environment in the Tarim Basin (NW China) and Their Reservoir Potential.” *Facies* 67: 25. https://doi.org/10.1007/s10347-021-00633-0.

Supporting Information

Additional supporting information can be found online in the Supporting Information section.